INSTITUTO POLITÉCNICO DE BRAGANÇA Escola Superior de Tecnologia e Gestão

CEFET/RJ

Estimation Of Transmission Line Parameters

EMMANUEL LOPES DA CRUZ SALDANHA

Dissertation presented to the School of Technology and Management of Bragança to obtain the Master's Degree in Renewable Energies ang Energy Efficiency within the scope of the joint diploma with CEFET/RJ.

Work oriented by:

Prof. Dra. Ângela P. Ferreira

Prof. Dra. Maria F. Pacheco

Prof. Dra. Cintia F. F. Carraro

Bragança
June of 2024

Dedico este trabalho à Deus, à minha família e aos meus amigos.

Bragança
Junho de 2024

Abstract

Transmission line parameters can change over time due to environmental variations and component aging. Traditional calculations of these parameters, based on geometrical data from manufacturers do not account for these dynamics, leading to inaccuracies that impact real-time system operations and long-term applications. This study explores two methods for estimating transmission line parameters. The first approach utilizes Kirchhoff's law and the characteristic equations of the equivalent π model of transmission lines along with phasor measurements to estimate the line parameters. The second method involves deriving the admittance matrix from sequential voltage and current phasor measurements for a fully observable power system. Two case studies are conducted in this work. One examines a five-bus radial network through the first approach and the other analyzes the IEEE 14-bus test case system through both methods. Series resistance and inductance were estimated with good accuracy by both methods, although the first method had higher accuracy. Shunt admittance was identified using the first approach, but the second approach was not capable of doing so and should be further investigated. Additionally, a sensitivity analysis showed that the number of available measurements impacts the accuracy of the second approach.

Keywords - transmission line parameter estimation; phasor measurement unit; power flow; state estimation; graph theory

Resumo

Os parâmetros das linhas de transmissão podem variar ao longo do tempo devido às mudanças ambientais e ao envelhecimento dos components das linhas. Os cálculos convencionais desses parâmetros, baseados na geometria das linhas, não consideram essas mudanças, resultando em imprecisões que afetam as operações em tempo real e as aplicações de longo prazo do sistema. Neste estudo, são explorados dois métodos para estimar os parâmetros da linha de transmissão. O primeiro método utiliza a lei de Kirchhoff e as equações características do modelo π equivalente das linhas de transmissão, juntamente com medições fasoriais, para realizar a estimative dos parâmetros das linhas. O segundo método envolve a obtenção da matriz admitância a partir de medições fasoriais de tensão e corrente para um sistema de potência totalmente observável. Dois estudos de caso são conduzidos, um em uma rede radial de cinco barras usando o primeiro método e outro no sistema de teste de 14 barras do IEEE empregando ambos os métodos. Tanto a resistência quanto a indutância em série foram estimadas com precisão por ambos os métodos, porém o primeiro método demonstrou maior precisão. Enquanto a admitância *shunt* foi identificada com sucesso usando o primeiro método, o segundo método não conseguiu estimá-la com eficácia e requer investigação adicional. Adicionalmente, uma análise de sensibilidade revelou que a precisão do segundo método é impactada pela quantidade de medições fasoriais disponíveis.

Palavras-chave - estimação de parâmetros de linhas de transmissão; *phasor measurement unit*; fluxo de potência; estimação de estados; teoria de grafos

Summary

Figure Index

Table Index

Abbreviations

DERs – Distributed energy resources

DSE - Dynamic state estimation

FACTS - Flexible alternating current transmission system

FASE - Forecasting-aided state estimation

GPS - Global positioning system

HVDC - High-voltage direct current

LAV - Least average value

LSE – Linear state estimation

MLE - Maximum likelihood estimation

PDC - Phasor data concentrator

PDF - Probability density function

PMU - Phasor measurement units

SCADA - Supervisory control and data acquisition

SSE - Static state estimation

TLPE - Transmission line parameters estimation

TLPI – Transmission line parameters identification

TSE - Tracking state estimation

μPMUs – Micro phasor measurement units

WLS – Weighted least squares

1. Introduction

The rise of distributed energy resources (DERs) foreshadows significant changes in the power system sector. Incorporating DERs brings about intricacies that require advanced measurement, communication, and control systems. Conventional power grids, initially built for centralized power generation, must adapt to manage the two-way power flows characteristic of DERs. This emphasizes the urgent requirement to improve the grid's operational intelligence for real-time monitoring and network topology management.

The characteristics of transmission lines can fluctuate over time due to alterations in environmental factors like temperature, soil resistivity, and the natural aging of line conductors and cables [1], [2], [3]. For example, underground cables experience a rise in line inductance over time as a result of tape shield corrosion, and an increase in line capacitance due to the deterioration of the dielectric constant of cable insulation caused by moisture and overheating from excessive loads [1].

Moreover, errors in manufacturing data, construction discrepancies, and misestimations of line lengths, compounded by other human-related influences, can lead to substantial inaccuracies in line parameters. Research indicates that discrepancies in line parameters recorded in databases may amount to as much as 30% of their true values [2], [3].

Mistakes in line parameters values have adverse effects on state estimation, operational control, reactive power optimization, line loss management, relay protection and configuration, event detection, and other critical functions [2], [3], [4], [5].

Hence, it can be stated that precise transmission line parameters are essential for all operational, control, and planning investigations in contemporary power systems, with their precision playing a direct role in ensuring the stable and secure functioning of the power grid [6], [7], [8].

The primary methods for transmission line parameters identification or estimation (TLPI or TLPE) depend on state estimation outcomes; however, the measurements utilized must fulfill observability criteria, which might not be achievable in every power system [4].

In modern power systems, the utilization of Supervisory Control and Data

Acquisition (SCADA) technology and Phasor Measurement Units (PMUs) is increasing due to the demand for enhanced real-time monitoring and control of the grid [3]. Their synchronized voltage and current phasor measurements, which include magnitudes and phase angles, enhance state estimation, with numerous TLPI techniques relying on these measurements [6], [7], [9]. However, installing a PMUs on every bus within a power system may not be cost-effective, and certain buses, particularly in distribution networks, may not have measurement devices at all [3], [4].

With that in mind, some TLPI techniques mix conventional and phasorial measurements and others explore alternatives for not fully observable power systems [10], [11].

1.1 Objective

This study aims to explore the estimation of transmission line parameters using the equivalent π model with lumped series resistance and reactance, along with shunt susceptance, utilizing real-time synchronized phasor measurements from both ends of the line. Furthermore, it involves an algorithm that calculates the admittance matrix from sequential voltage and current phasor measurements, following the method presented in [10] for a fully observable power system. This algorithm is applied and evaluated in a case study built on the IEEE 14-bus test system. A review of the classical approach to the calculation of transmission line parameters and some of the major technologies used in TLPI like PMU, graph theory and state estimation is also made.

1.2 Structure Of The Work

This work is organized as follows: Chapter 2 explores the state of the art of line parameters calculation, first introducing the classical calculation of line parameters then doing a review of modern TLPI and major technologies associated with it. Chapter 3 presents the methodologies developed in this work. Chapter 4 introduces the case studies constructed to assess the methodologies and Chapter 5 presents and discusses the results. Finally, Chapter 6 rounds out the work with the conclusion.

Noteworthy, as a result of this work, a paper was presented at the Mediterranean Smart Cities Conference of 2024 [12].

2. State Of The Art

Resistance, inductance, capacitance, and conductance are the parameters that characterize a transmission line. The resistance and inductance uniformly distributed along the line forms the series impedance and the conductance and capacitance between conductors (single-phase line) or from a conductor to neutral (three-phase line) form the shunt admittance.

The following topics present the classical way of calculating these parameters based in line geometry and modelling. There are three line models classified by the length of the line, the short model, the π nominal model and the π equivalent model.

After presenting the line models and classical line parameters calculation, transmission line parameter estimation is introduced and studies on the matter are reviewed. Also, key technologies and concepts related to TLPE are discussed.

2.1 Classical Modeling And Calculation Of Transmission Lines Parameters

2.1.1 Transmission Line Models

Depending on the length of the line, some simplifications can be made when representing the line. That is the case for short and medium length lines. These lines models use lumped parameters modeling that still represents the real line with good accuracy.

A short line is no longer than 80 km and a medium line length varies between 80 km and 240 km. Long lines are longer than 240 km and require calculations in terms of distributed constants for a high accuracy, but in some cases a lumped parameter approximation can be used for lines up to 320 km in length [13].

The next subtopics present the models and their associated equations.

2.1.1.1 SHORT LINE MODELING

For short lines, the shunt capacitance is omitted because of how small it is. This results in minimal to no loss of accuracy.

The series resistance and inductance for the total length of the line are considered on this representation and shown in Figure 1.

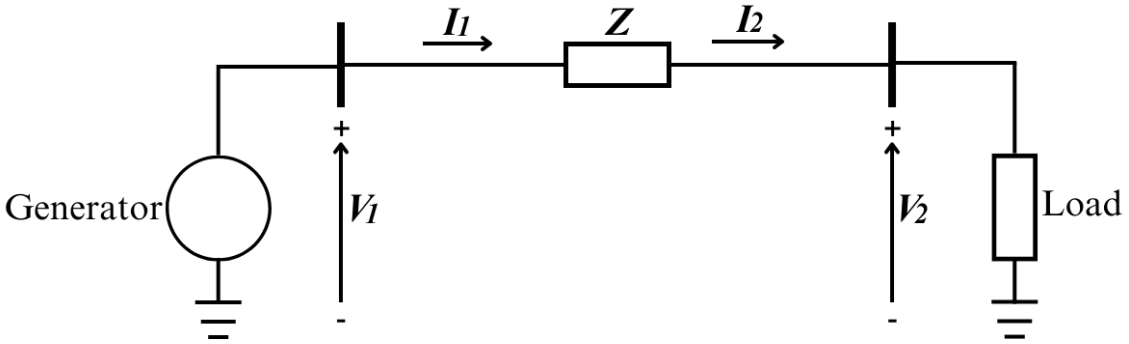

Figure 1- Representation of a short transmission line.

In this model, the sending and receiving end currents, I_1 and I_2, respectfully, are equal and the circuit is solved as a simple series ac circuit

$$V_1 = V_2 + I_2 Z \tag{2.1}$$

where V_1 is sending end voltage, V_2 is the receiving end voltage and Z is the lumped series impedance.

2.1.1.2 Medium Line Modeling

For medium-length transmission lines, the shunt admittance is considered in modeling. If the total shunt admittance Y_{sh} is divided equally into two parts placed at the sending and receiving ends of the line, we obtain the nominal π representation as in Figure 2.

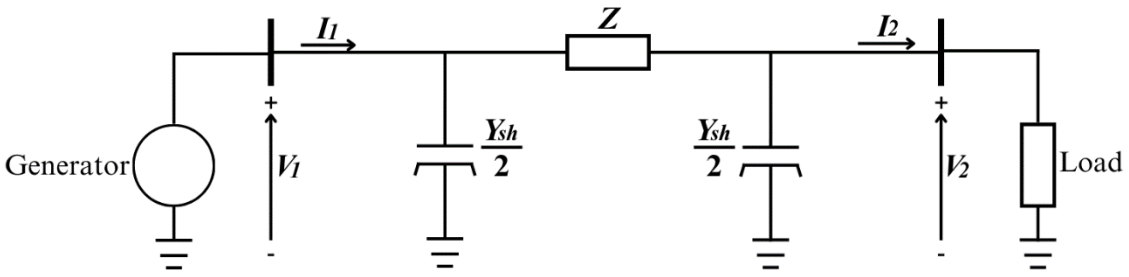

Figure 2- Nominal π representation of a medium transmission line.

This representation is characterized by four generalized circuit constants called A, B, C and D. These constants are obtained by the equations expressing V_1 and I_1

$$V_1 = \left(\frac{ZY_{sh}}{2} + 1\right)V_2 + ZI_2 = AV_2 + BI_2 \tag{2.2}$$

$$I_1 = \left(\frac{ZY_{sh}}{4} + 1\right)V_2 Y_{sh} + \left(\frac{ZY_{sh}}{2} + 1\right)I_2 = CV_2 + DI_2 \tag{2.3}$$

These constants apply to any linear, passive, and bilateral four-terminal network having two pairs of terminals (two-port network), but they vary according to the network configuration.

2.1.1.3 Long Line Modeling

Modeling long transmission lines requires taking in consideration that the parameters of the line are distributed uniformly throughout the length of the line. Every little section of length *dx* in the line positioned at a distance *x* from the receiving end of the line has a series impedance *zdx* and a shunt admittance *ydx* and phasors of voltage dV and current dI that vary with *x* as shown in Figure 3.

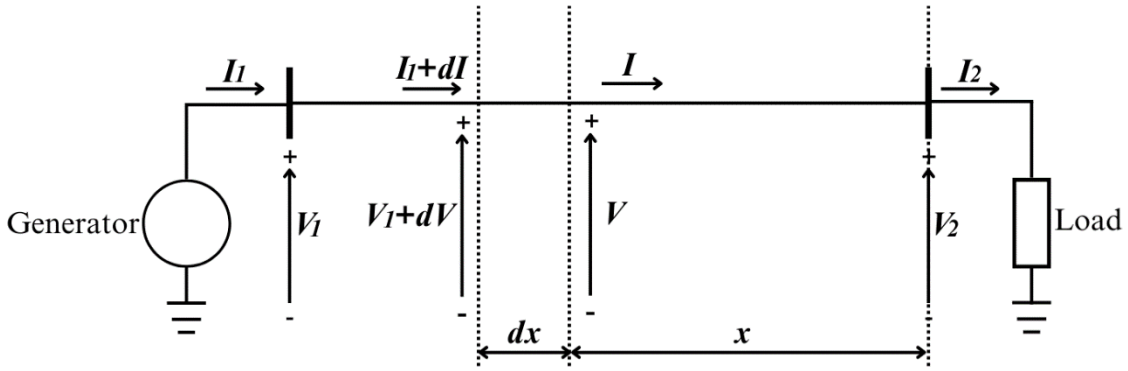

Figure 3- Representation of a section *dx* of a long line and the voltage and current phasors associated with it.

The rms values and phase angles of voltage V and current I at any specified point along the line can be obtained in terms of the distance *x* from the receiving end to the specified point, provided that the voltage and current at the receiving end of the line and the parameters of the line are known. This is expressed by the following equations:

$$V = \frac{V_2 + I_2 Z_C}{2}\varepsilon^{\gamma x} + \frac{V_2 - I_2 Z_C}{2}\varepsilon^{-\gamma x} \tag{2.4}$$

$$I = \frac{V_2/Z_C + I_2}{2}\varepsilon^{\gamma x} - \frac{V_2/Z_C - I_2}{2}\varepsilon^{-\gamma x} \tag{2.5}$$

where $Z_C = \sqrt{z/y}$ is the characteristic impedance of the line, $\gamma = \sqrt{zy}$ is the propagation constant of the line, *z* is the series impedance per unit length per phase and *y* is the shunt admittance per unit length per phase to neutral.

These equations are often presented in hyperbolic form due to reflection of voltage and current waves in the line, as follows:

$$V = V_2 \cosh(\gamma x) + I_2 Z_C \sinh(\gamma x) \tag{2.6}$$

$$I = I_2 \cosh(\gamma x) + \frac{V_2}{Z_C} \sinh(\gamma x) \tag{2.7}$$

And letting $x = l$ to obtain the voltage and current at the sending end, the generalized circuit constants are also obtained

$$V_1 = V_2 \cosh(\gamma l) + I_2 Z_C \sinh(\gamma l) = V_2 A + I_2 B \tag{2.8}$$

$$I_1 = I_2 \cosh(\gamma l) + \frac{V_2}{Z_C} \sinh(\gamma l) = I_2 D + V_2 C \tag{2.9}$$

An approximation of the nominal π can be made for long lines and is called equivalent π model. The equivalent π model is shown in Figure 4.

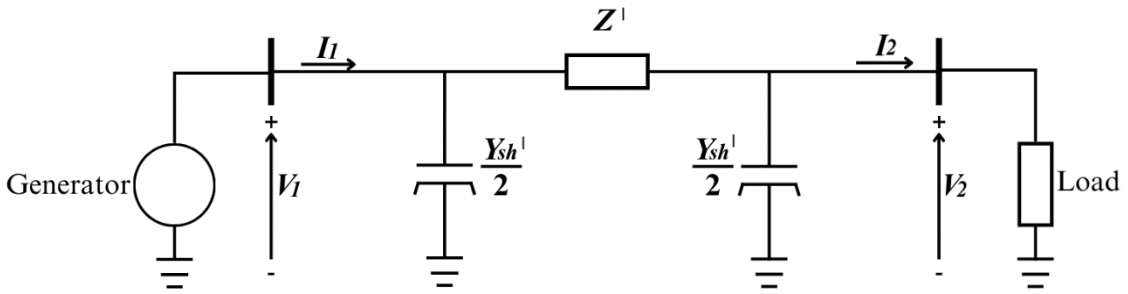

Figure 4- The equivalent π model of a transmission line.

where Z' is

$$Z' = Z_c \sinh(\gamma l) = Z \frac{\sinh(\gamma l)}{\gamma l} \tag{2.10}$$

and $\frac{Y'}{2}$ is

$$\frac{Y'}{2} = \frac{1}{Z_c} \tanh\left(\frac{\gamma l}{2}\right) = \frac{Y}{2} \frac{\tanh(\gamma l/2)}{\gamma l/2} \tag{2.11}$$

2.1.2 Classical Line Parameters Calculation

Knowing the parameters considered for each transmission line model, the following topics detail the classical methods of calculation of line resistance, inductance,

conductance, and capacitance.

2.1.2.1 Resistance

The resistance directly associated with power loss in the line is called effective resistance. It is equivalent to the dc resistance if the current distribution throughout the line conductor is uniform. In that case, the resistance, *R,* can be calculated based on the resistivity of the conductor, ρ, the length of the line, *l,* and the cross-section area of the conductor, *A*

$$R = \frac{\rho l}{A} \tag{2.12}$$

however, the resistance of a metallic conductor varies linearly with the variation of temperature and thus the resistance of the line changes during the day.

Figure 5 shows the variation of resistance with the variation of temperature *T*.

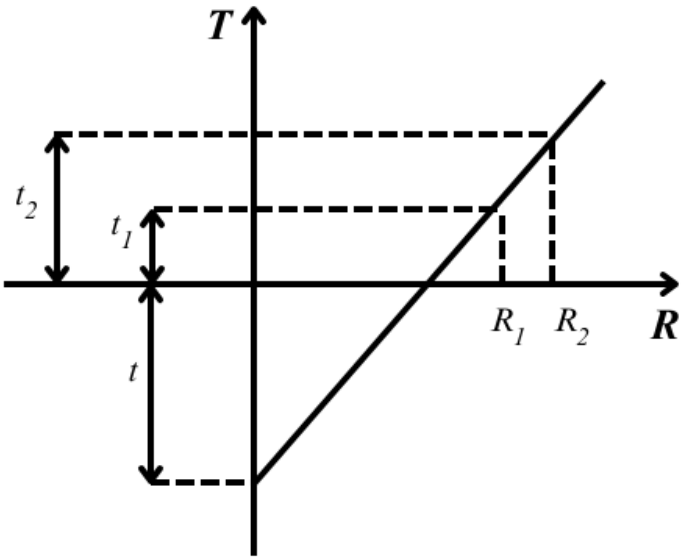

Figure 5 – Resistance varying with temperature.

Figure 5 can be used to correct resistance changes due to temperature variation by expressing the relation between known resistances at given temperatures and the point *t* that represents the constant of the material

$$\frac{R_2}{R_1} = \frac{t + t_2}{t + t_1} \tag{2.13}$$

However, temperature is not the only factor that influences resistance variation. The increase of current frequency also impacts the resistance of the line as it alters current

density uniformity in a phenomenon called *skin effect*, where current density is higher on the surface of the conductor than on the interior. This causes a higher effective resistance.

Aware of resistance variation due to the factors mentioned, manufacturers inform tabled electrical characteristics of their conductors, but this information becomes obsolete with time because of aging of the materials and other causes.

2.1.3 Inductance

As for the inductance L of the transmission line, its value is related to the flux linkages λ inside and outside the conductors and the configuration of the transmission lines affects the final value. Single phase lines with two wires, lines with grouped conductors, composite-conductor lines, three phase lines with equilateral or unsymmetrical spacings all have different geometries, and this affects the flux linkages and the inductance.

The inductance of a conductor due to its internal flux is defined as

$$L = \frac{\lambda}{I} \tag{2.14}$$

where I is the phasorial current circulating in the conductor.

For an initial deduction of the flux linkage outside a conductor, assume a group of n conductors, each one placed at a given distance from a remote point P, each distance being represented by $D_{1P}, D_{2P} ... D_{nP}$ as Figure 6 shows.

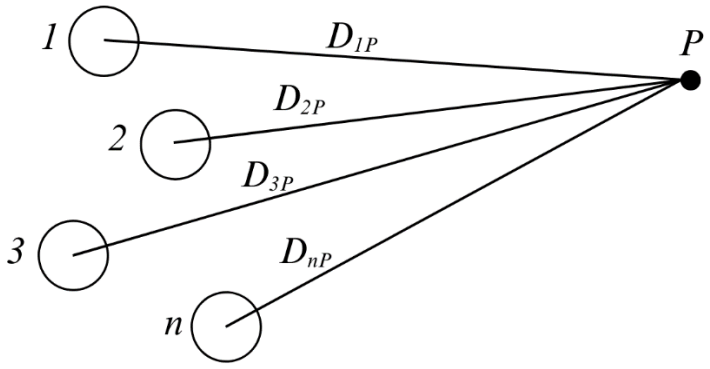

Figure 6 – Group of n conductors distant from a remote point P.

All conductors from Figure 6 carry current and the sum of all the currents is zero. Every conductor in the group has a flux linkage to point P due to the current it is carrying. For conductor one, this flux linkage is expressed by

$$\lambda_{1P1} = \left(\frac{I_1}{2} + 2I_1 \ln\left(\frac{D_{1P}}{r_1} \right) \right) \times 10^{-7} = 2 \times 10^{-7} I_1 \ln\left(\frac{D_{1P}}{r_1^{'}} \right) \tag{2.15}$$

where $r_1^{'} = r_1 \varepsilon^{-1/4}$. The 10^{-7} multiplying factor appears due to considering a constant and unitary relative permeability of the conductor's material.

In addition, there are flux linkages between conductor one and every other conductor in the group due to their internal current. For example, the flux linkage between conductor one and conductor two due to the current flowing in conductor two is equal to the flux produced by the current in conductor two between the point *P* and conductor one.

$$\lambda_{1P2} = \left(I_2 \ln\left(\frac{D_{2P}}{D_{12}} \right) \right) 2 \times 10^{-7} \tag{2.16}$$

Thus, the total flux linkage between conductor one and point *P* considers the flux linkages relative to all other conductors in the group and is expressed by

$$\lambda_{1P} = 2 \times 10^{-7} \left(I_1 \ln\left(\frac{D_{1P}}{r_1^{'}} \right) + I_2 \ln\left(\frac{D_{2P}}{D_{12}} \right) + I_3 \ln\left(\frac{D_{3P}}{D_{13}} \right) + ... + I_n \ln\left(\frac{D_{nP}}{D_{1n}} \right) \right) \tag{2.17}$$

Knowing that the sum of all currents is zero and doing some mathematical substitutions, the equation above is rearranged in

$$\lambda_{1P} = 2 \times 10^{-7} \left(\begin{array}{l} I_1 \ln\left(\frac{1}{r_1^{'}} \right) + I_2 \ln\left(\frac{1}{D_{12}} \right) + I_3 \ln\left(\frac{1}{D_{13}} \right) + ... + I_n \ln\left(\frac{1}{D_{1n}} \right) \\ + I_1 \ln\left(\frac{D_{1P}}{D_{nP}} \right) + I_2 \ln\left(\frac{D_{2P}}{D_{nP}} \right) + I_3 \ln\left(\frac{D_{3P}}{D_{nP}} \right) + ... + I_{n-1} \ln\left(\frac{D_{(n-1)P}}{D_{nP}} \right) \end{array} \right) \tag{2.18}$$

Finally, if point P is located at an exceedingly long distance from the conductors, the terms related to logarithmic ratios of distances from P becomes infinitesimal and the flux linkage is given by

$$\lambda_1 = 2 \times 10^{-7} \left(I_1 \ln\left(\frac{1}{r_1^{'}} \right) + I_2 \ln\left(\frac{1}{D_{12}} \right) + I_3 \ln\left(\frac{1}{D_{13}} \right) + ... + I_n \ln\left(\frac{1}{D_{1n}} \right) \right) \tag{2.19}$$

the above equation gives the flux linkages of conductor 1 in a group of conductors where the sum of all currents is zero. The expression for the other conductors in the group are analogous to this equation.

This result can be applied to a balanced three-phase line like the one shown in Figure 7, where the distance *D* between each pair of conductors is equal.

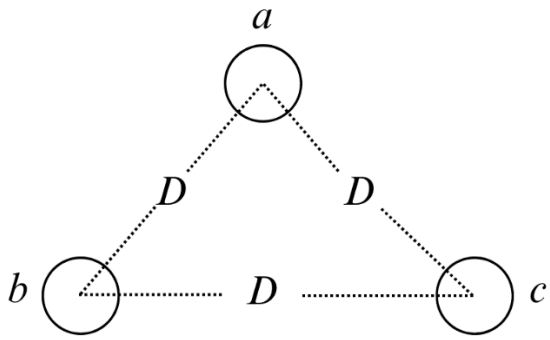

Figure 7 – Equally spaced three-phase line.

The flux linkage for conductor *a*, representing phase *a*, of Figure 7 is

$$\lambda_a = 2\times10^{-7}\left(I_a \ln\left(\frac{1}{D_s}\right) + I_b \ln\left(\frac{1}{D}\right) + I_c \ln\left(\frac{1}{D}\right)\right) \tag{2.20}$$

where D_s is the *geometric mean radius* of the conductor. As the phases are balanced, $I_a = -\left(I_b + I_c\right)$ and equation 6 can be rearranged as

$$\lambda_a = 2\times10^{-7}\left(I_a \ln\left(\frac{1}{D_s}\right) - I_a \ln\left(\frac{1}{D}\right)\right) = 2\times10^{-7}\left(I_a \ln\left(\frac{D}{D_s}\right)\right) \tag{2.21}$$

and, finally, using the relation given by (2.14) the inductance of conductor *a* is

$$L_a = 2\times10^{-7} \ln\left(\frac{D}{D_s}\right) \tag{2.21}$$

Because of the symmetry of the line, the inductance of conductors *b* and *c* is the same as the inductance of conductor *a*.

However, there are cases where the line is not equally spaced and consequently the flux linkages and inductances of each phase are not equal, and the circuit is unbalanced. Transposition of the conductors is a way to balance the phases.

Transposition is the name given to the process of exchanging the positions of the conductors at regular intervals along the line (cycles) so that each conductor occupies the original position of every other conductor over an equal distance [13]. As a result, each conductor has the same average inductance over the whole transposition cycle.

Figure 8 represents the transposition cycle of line. The positions each phase *a*, *b* and *c* of the line occupy over time are numbered as 1, 2 and 3.

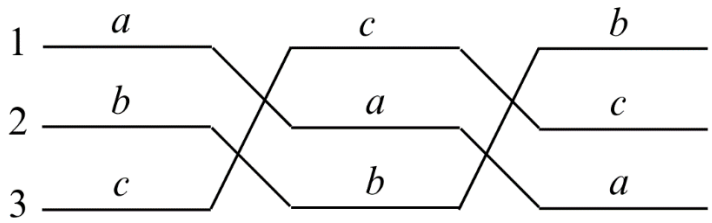

Figure 8 – Transposition of a three-phase line.

When a line is transposed, to obtain the average inductance of the conductors it is necessary to calculate the average flux linkage, meaning that the flux linkage of the conductor at every position it occupied must be calculated.

The equations below calculate the flux linkage of the conductor *a* of Figure 8 at positions 1, 2 and 3.

$$\lambda_{a1} = 2\times10^{-7}\left(I_a \ln\left(\frac{1}{D_s}\right) + I_b \ln\left(\frac{1}{D_{12}}\right) + I_c \ln\left(\frac{1}{D_{31}}\right)\right) \tag{2.23}$$

$$\lambda_{a2} = 2\times10^{-7}\left(I_a \ln\left(\frac{1}{D_s}\right) + I_b \ln\left(\frac{1}{D_{23}}\right) + I_c \ln\left(\frac{1}{D_{12}}\right)\right) \tag{2.24}$$

$$\lambda_{a3} = 2\times10^{-7}\left(I_a \ln\left(\frac{1}{D_s}\right) + I_b \ln\left(\frac{1}{D_{31}}\right) + I_c \ln\left(\frac{1}{D_{23}}\right)\right) \tag{2.25}$$

Thus, adding (2.23), (2.24) and (2.25) and calculating the average, the average flux linkage for conductor *a* is

$$\lambda_a = \frac{\lambda_{a1}+\lambda_{a2}+\lambda_{a3}}{3} = \frac{\left(2\times10^{-7}\right)}{3}\left(3I_a \ln\left(\frac{1}{D_s}\right) + I_b \ln\left(\frac{1}{D_{12}D_{23}D_{31}}\right) + I_c \ln\left(\frac{1}{D_{12}D_{23}D_{31}}\right)\right) \tag{2.26}$$

and as after transposing the line the circuit is balanced, $I_a = -\left(I_b + I_c\right)$ is true and (2.26) can be rearranged as

$$\lambda_a = \frac{\left(2\times10^{-7}\right)}{3}\left(3I_a \ln\left(\frac{1}{D_s}\right) - I_a \ln\left(\frac{1}{D_{12}D_{23}D_{31}}\right)\right) \tag{2.27}$$

$$\lambda_a = 2\times10^{-7}\left(I_a \ln\left(\frac{\sqrt[3]{D_{12}D_{23}D_{31}}}{D_s}\right)\right) \tag{2.28}$$

and the average inductance of conductor *a* can be obtained by

$$L_a = 2\times10^{-7}\ln\left(\frac{D_{eq}}{D_s}\right) \tag{2.29}$$

where $D_{eq} = \sqrt[3]{D_{12}D_{23}D_{31}}$.

After transposing the phases, the average inductance of conductor *a* is equal to that of conductors *b* and *c*, so this final equation gives the average inductance per phase of the line.

2.1.4 Conductance And Capacitance

Conductance usually has a minimal contribution to shunt admittance and because of it is often neglected.

On the other hand, the capacitance depends on the size and spacing of the conductors and increases with the length of the lines, affecting the voltage drop along the lines as well as efficiency and power factor of the line and the stability of the system of which the line is a part. The geometry of the lines also influences on the capacitance.

The capacitance of a transmission line is the result of the potential difference between the conductors. This potential difference causes them to be charged in the same manner as the plates of a capacitor when there is a potential difference between them.

Gauss law for electric fields says that the total electric charge within a closed surface equals the total electric flux emerging from the surface. This means that in a cylindrical surface that is concentric with a conductor the electric flux density D_f on the surface is equal to the charge *q* on the conductor in coulombs per meter of length divided by the area of the surface and the *x* distance in meters from the conductor to the surface

$$D_f = \frac{q}{2\pi x} \tag{2.29}$$

The electric field intensity at *x* is equal to the electric flux density divided by the permittivity *k* of the medium where the conductor lies

$$E = \frac{q}{2\pi xk} \tag{2.30}$$

This electric field intensity is used to compute the difference in potential between two points P_1 and P_2 like the ones represented in Figure 9, where *q* is the charge of the

cylindrical conductor and D_1 and D_2 are the distances between point P_1 and the conductor and point P_2 and the conductor, respectively.

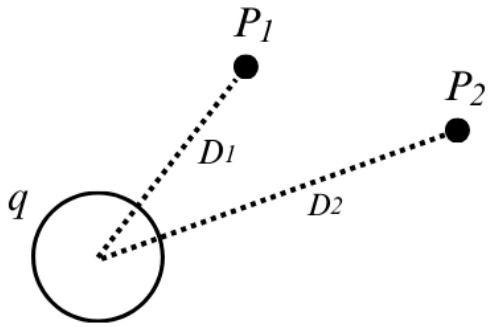

Figure 9- Two points near a cylindrical conductor.

Considering two equipotential surfaces concentric with the conductor in Figure 9 passing through points P_1 and P_2, the difference in potential v_{12} between the points can be calculated by integrating the field intensity over a radial path between the equipotential surfaces

$$v_{12} = \int_{D_1}^{D_2} E dx = \int_{D_1}^{D_2} \frac{D_f}{k} dx = \int_{D_1}^{D_2} \frac{q}{2\pi x k} dx = \frac{q}{2\pi k} \ln\left(\frac{D_2}{D_1}\right) \tag{2.31}$$

Applying this to the three-phase line from Figure 7, the difference in potential v_{ab} due to the charges on conductors *a* and *b* is

$$v_{ab} = \frac{1}{2\pi k}\left(q_a \ln\left(\frac{D}{r}\right) + q_b \ln\left(\frac{r}{D}\right)\right) \tag{2.32}$$

where *r* is the radius of the conductors and *D* the distance between the conductors.

This difference in potential between *a* and *b* is also influenced by the charge in conductor *c* and it is expressed by

$$v_{ab} = \frac{q_c}{2\pi k} \ln\left(\frac{D}{D}\right) \tag{2.33}$$

However, *c* is equidistant to *a* and *b*, thus the difference in potential due only to

the charge in c is zero, as represented by the factor $\ln\left(\frac{D}{D}\right)$, and could be ignored. The same applies to the influence of the charge in b to the voltage between a and c and the influence of the charge in a to the voltage between b and c.

Nonetheless, for mathematical purposes, considering the effect of all three charges to the difference in potentials v_{ab} and v_{ac}, there is

$$v_{ab} = \frac{1}{2\pi k}\left(q_a \ln\left(\frac{D}{r}\right) + q_b \ln\left(\frac{r}{D}\right) + q_c \ln\left(\frac{D}{D}\right)\right) \tag{2.34}$$

$$v_{ac} = \frac{1}{2\pi k}\left(q_a \ln\left(\frac{D}{r}\right) + q_b \ln\left(\frac{D}{D}\right) + q_c \ln\left(\frac{r}{D}\right)\right) \tag{2.35}$$

Adding the above equations and doing $-q_a = q_b + q_c$ as the sum of the charges on the three conductors is zero

$$v_{ab} + v_{ac} = \frac{3q_a}{2\pi k}\ln\left(\frac{D}{r}\right) \tag{2.36}$$

Phasors give the following relation between line voltages and line to neutral

$$v_{ab} + v_{ac} = 3v_{an} \tag{2.37}$$

and substituting (2.37) in (2.36)

$$v_{an} = \frac{q_a}{2\pi k}\ln\left(\frac{D}{r}\right) \tag{2.38}$$

therefore, finally, since capacitance to neutral is the ratio of the charge on a conductor to the voltage between that conductor and neutral

$$C_n = \frac{q_a}{v_{an}} = \frac{2\pi k}{\ln(D/r)} \tag{2.39}$$

This equation expresses the capacitance to neutral for an equilaterally spaced three-phase lines.

For three-phase lines with unsymmetrical spacing, a process like calculating flux

linkages for transposed lines is done, meaning that an average capacitance to neutral for each conductor is calculated and expressed by

$$C_n = \frac{2\pi k}{\ln\left(D_{eq}/r\right)} \tag{2.40}$$

where $D_{eq} = \sqrt[3]{D_{12}D_{23}D_{31}}$ represents the equivalent diameter of the bundled conductors.

But a more complete calculation should take in consideration the effect of the earth on the capacitance of the lines because it alters the electric fields of the charged conductors. The earth can be seen as a perfect conductor shaped horizontal and infinite in length, but the irregularities of the terrain and type of surface limits the assumption of a plain and equipotential surface.

For calculations, earth can be replaced by an imaginary conductor charged equally in magnitude and opposite in sign to that of the original conductor. This imaginary conductor is placed below the surface of the earth by the same distance the real conductor is above the surface. This method of calculating capacitance is called method of images.

Figure 10 presents an example of a three-phase line with its imaginary conductors below the surface of the earth. The real conductors occupy the positions 1, 2 and 3 of the transposition cycle and have charges q_a, q_b and q_c, respectively. The imaginary conductors occupy the same positions but are placed below ground and have opposite charges $-q_a$, $-q_b$ and $-q_c$, respectively. D_{12}, D_{23} and D_{31} are the distances between the real conductors and H_1, H_2 and H_3 are the distances between each conductor and it's imaginary counterpart. H_{12}, H_{23} and H_{31} represent the distances between the pairs of real and imaginary conductors.

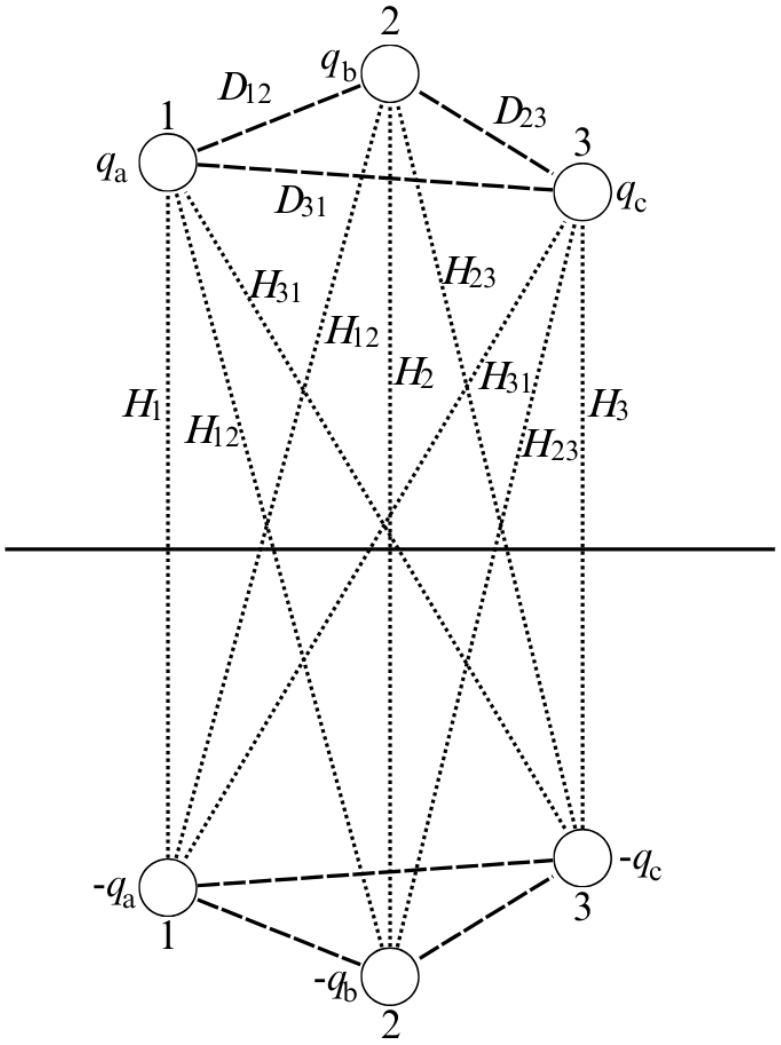

Figure 10- Three-phase line and its image.

The method of images considers a transposed line and that conductors a, b and c carry the charges q_a, q_b and q_c and occupy positions 1, 2, and 3, respectively, in the first part of the transposition cycle as Figure 10 shows. The difference in potential between a and b considering the three charges and their images is

$$v_{ab} = \frac{1}{2\pi k}\left[\begin{array}{l} q_a\left(\ln\left(\frac{D_{12}}{r}\right)-\ln\left(\frac{H_{12}}{H_1}\right)\right)+q_b\left(\ln\left(\frac{r}{D_{12}}\right)-\ln\left(\frac{H_2}{H_{12}}\right)\right) \\ +q_c\left(\ln\left(\frac{D_{23}}{D_{31}}\right)-\ln\left(\frac{H_{23}}{H_{31}}\right)\right) \end{array}\right] \tag{2.41}$$

Equations for v_{ab} can be written for each part of the transposition cycle, assuming constant charge per unit length of each conductor. This allows us to obtain the average

value of the phasor v_{ab}. The equation for the average value of the phasor v_{ac} is found in a similar manner, and 3 v_{an} is obtained by adding the average values of v_{ab} and v_{ac}. Knowing that the sum of the charges is zero, the capacitance to neutral is expressed by

$$C_n = \frac{2\pi k}{\ln\left(\frac{D_{eq}}{r}\right) - \ln\left(\frac{\sqrt[3]{H_{12}H_{23}H_{31}}}{\sqrt[3]{H_1H_2H_3}}\right)} \tag{2.42}$$

Comparing this equation to the equation that expresses the capacitance to neutral for three-phase lines with unsymmetrical spacing shows that earth increases the capacitance of the line. However, for high conductors above ground, the correction term represented by $\ln\left(\frac{\sqrt[3]{H_{12}H_{23}H_{31}}}{\sqrt[3]{H_1H_2H_3}}\right)$ is small due to nearly equal diagonal and vertical distances in the numerator and denominator. This is typically the case, and the ground effect is usually ignored for three-phase lines, except in symmetrical component calculations when the sum of the three line currents is not zero [13].

2.2 Transmission Line Parameters Estimation

In the classical approaches, transmission line parameters are calculated from the geometry of the line conductors and the length of the lines or directly measured using specific instruments during the construction or maintenance of the transmission lines [6], [8], [9].

However, these methods are inaccurate due to simplified ideal models or inconvenient because they can only be utilized when the line is out of service [8].

Currently, supervisory control and data acquisition technology and phasor measurement units are being employed in modern power systems because of the need for more efficient real-time monitoring and control of the grid [3] and many transmission line parameter identification methods are based on these measurement systems and state estimation [1], [2], [6], [7], [9].

In fact, most recent studies focus on PMU measurements, developing methodologies and studying strategies to mitigate the negative impacts of inaccuracies in the PMU based measurement chain [2], [5], [8], [9], [14], [15], [16], [17].

However, as in a real electric power system PMU measurements may not be available due to factors such as cost of installation and observability of the network, there

are studies on mixed PMU and SCADA measurements for TLPI [3], [6] and methodologies based on topological analysis, power flow studies and data-driven regression that can be applied when phasor measurements are not available at all [10], [11], [18].

These techniques represent an advantage when compared to classical approaches, but their accuracy not only depends on their convergence but also on the accuracy of the measurement system and state estimation [1], [9].

Conventional TLPI techniques explore Kirchhoff's and Ohm's laws and transmission line models - usually the equivalent π model - to establish and solve nonlinear equations in terms of the line parameters and measurements of the power network [1], [2], [3], [10], [19], [20], [21]. Popular techniques to solve these nonlinear equations use waited least squares state estimation [22], [23], [24] and augmented state estimation [2], [25], [26], [27]. There are also TLPI studies based on residual sensitivity analysis [28], [29], [30] and the Newton-Raphson method [31], [32], [33].

Interesting recent studies [10], [11], [18] have linked power network topology identification and line parameter estimation.

Shi [18] studied an integrated estimation method based on linear regression and topological characteristics is proposed to obtain line parameters, topology, and phase specifications in distribution networks without micro phasor measurement units (μPMUs). Simulations are performed for both single-phase and three-phase networks and the result suggests that the proposed framework can provide accurate estimation results even with limited measurements.

Zhang [11] proposed a numerical method to identify the topology and estimate line parameters without the information of voltage angles given by PMUs is proposed in a two-step framework. The process begins by using a data-driven regression method to make an initial estimation of the topology and line parameter. This is followed by employing a joint data-and-model-driven method, specifically a specialized Newton-Raphson iteration and power flow equations, to calculate the line parameter, restore voltage angle, and make additional corrections to the topology.

Yuan [10] present a method for solving an inverse power flow issue where the nodal admittance matrix is estimated from voltage and current phasors collected at various bus locations. The study demonstrates that the admittance matrix can be distinctly characterized by a series of measurements taken during various stable system conditions,

provided that each bus has a measuring instrument. Additionally, for a radial power system, a Kron-reduced admittance matrix is derived even in cases where certain nodes in the system are not monitored (hidden nodes).

The study showcased in [10] is particularly interesting because it explores graph theory. In electrical engineering, graph theory is known for its application on optimal PMUs placement, state estimation and more activities related to the control and operation of electrical power systems [27], [34], [35].

Therefore, the next subsections further elaborate on three major technologies and techniques at use in TLPI: PMU/SCADA measurement systems, state estimation and graph theory.

2.2.1 PMU/SCADA

The PMU is an equipment that calculates both the magnitude and angle of the current and voltage from the buses it is connected to and by employing PMUs it's possible to obtain the full observability of the power system [36].

Although the first PMU model dates back to 1980, it is a trending technology in a world where the continuous increase in energy demand, high proliferation of intermittent renewable resources and the undergoing transition from traditional passive networks, which had unidirectional power flow, to active networks with bidirectional power flow and highly dynamic characteristics makes power system control and monitoring more challenging [36], [37], [38].

Figure 11 shows the first experimental PMU.

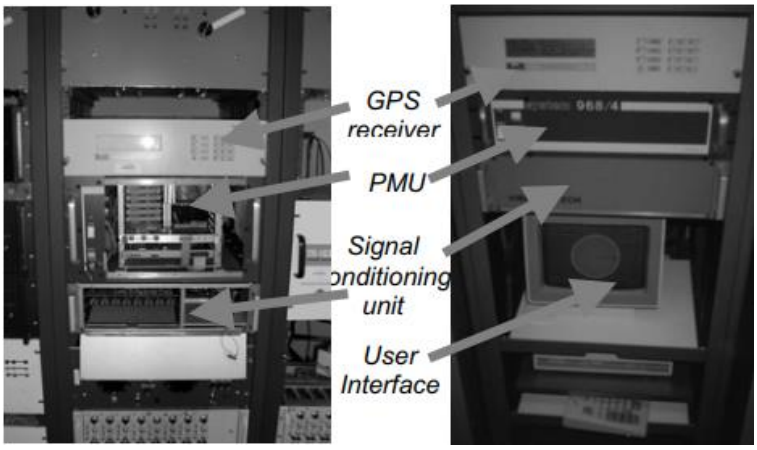

Figure 11- The first experimental PMU, developed at Virginia Tech in 1980 [39].

As shown in Figure 11, PMU relies on Global Positioning System (GPS) to

produce time traceable data, but the device is composed by some other elements too. The construction of a PMU is better shown in Figure 12.

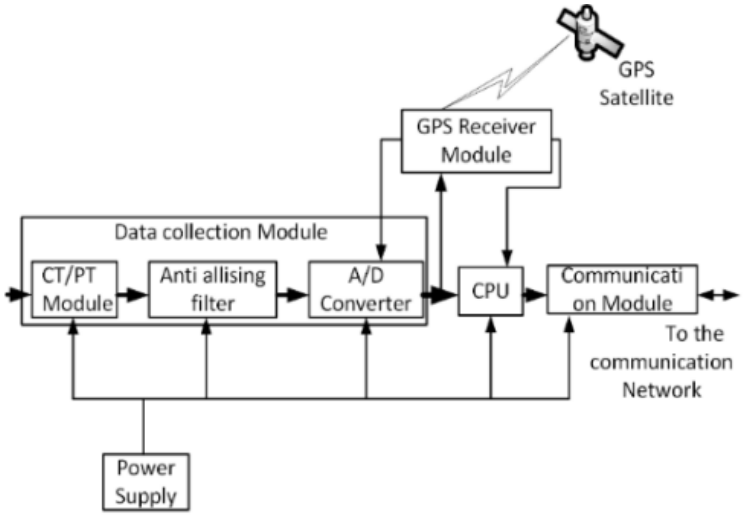

Figure 12- Block diagram of a PMU [37].

As Figure 12 illustrates, a PMU is composed by a GPS receiver module, a data collection module, a CPU, a communication module, and a power supply. At the data collection module, current and power transformers data go through an anti-aliasing filter that limits the signal bandwidth and then through an analog to digital converter where the desired digital signal is obtained. Then, the CPU computes the magnitude and phase of the currents and voltages and data time is synchronized with respect to the signal from the GPS receiver [37], [38].

With several PMUs installed, it is usual to have all phasor measurements transmitted to a Phasor Data Concentrator (PDC) which provides visualization of gathered and archived data and also do analytic functions [37], [40], as shows Figure 13.

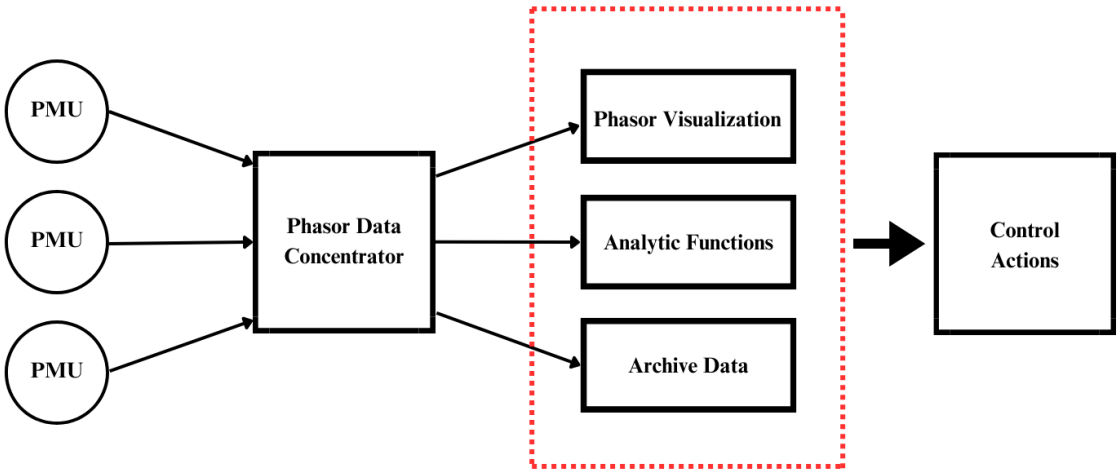

Figure 13- The use of PDC with multiple PMUs.

Figure 14 shows an example of a commercial PMU, model RES670 manufactured by Hitachi.

Figure 14- PMU model RES670 by Hitachi [41].

PMUs typically operate at a high sampling rate of 30/50/60 samples per second, but some PMUs built specifically to operate in distribution networks (μPMUs) can operate in a range that goes from 10 to 120 samples per second [38], [42].

PMUs are high precision equipment and provides real-time synchronized measurement, synchronized frequency, rate of change of frequency of voltage, current phasor quantities and their magnitude with an error of $\pm 1^{\circ}$ or $\pm 1\%$ [43].

Nevertheless, these devices are costly. Consequently, there have been studies focused on finding the best locations for PMU placement. These studies aim to provide an approach for achieving complete observability of the power system without requiring PMUs at every grid station [43], [44].

2.2.1.1 Usage Of PMU Around The World

China and Mexico make use of this technology since the decade of 1990, with China having installed around 3000 PMU units in its power grid nowadays, but Canada, The United States of America, Brazil, Russia and Europe are also references in phasor measurement units deployment [36].

Figure 15 shows the installed PMU in The United States of America and part of Canada until March of 2014.

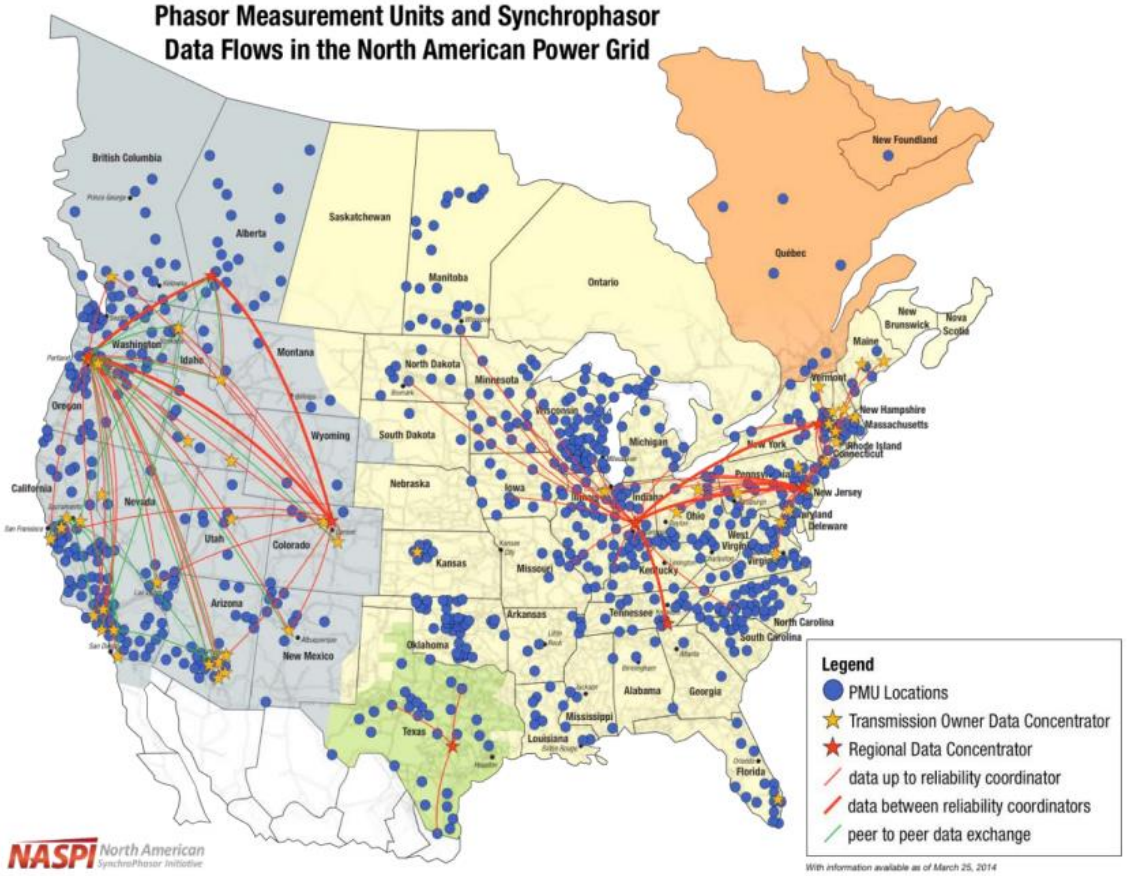

Figure 15- PMU installed in the north american power grid until March of 2014 [45].

In Figure 15 the blue dots represent PMU locations, the yellow stars represent transmission owner data concentrators, the red stars represent regional data concentrators, the yellow lines represent data up to reliability coordinators, the red lines represent data between reliability coordinators and the green lines represent peer to peer data exchange. The figure shows the location of 1700 PMUs, but nowadays the number of PMUs in use have increased to 2500 units [46].

India is also investing in PMU and have installed 66 units integrated through a

regional phasor data concentrator in a pilot project that aims to gather data from crucial points of the Indian power system like power plants, load dispatch centers and high-voltage direct current (HVDC) substations [40].

Figure 16 shows the installed PMUs in the Indian regional power grids.

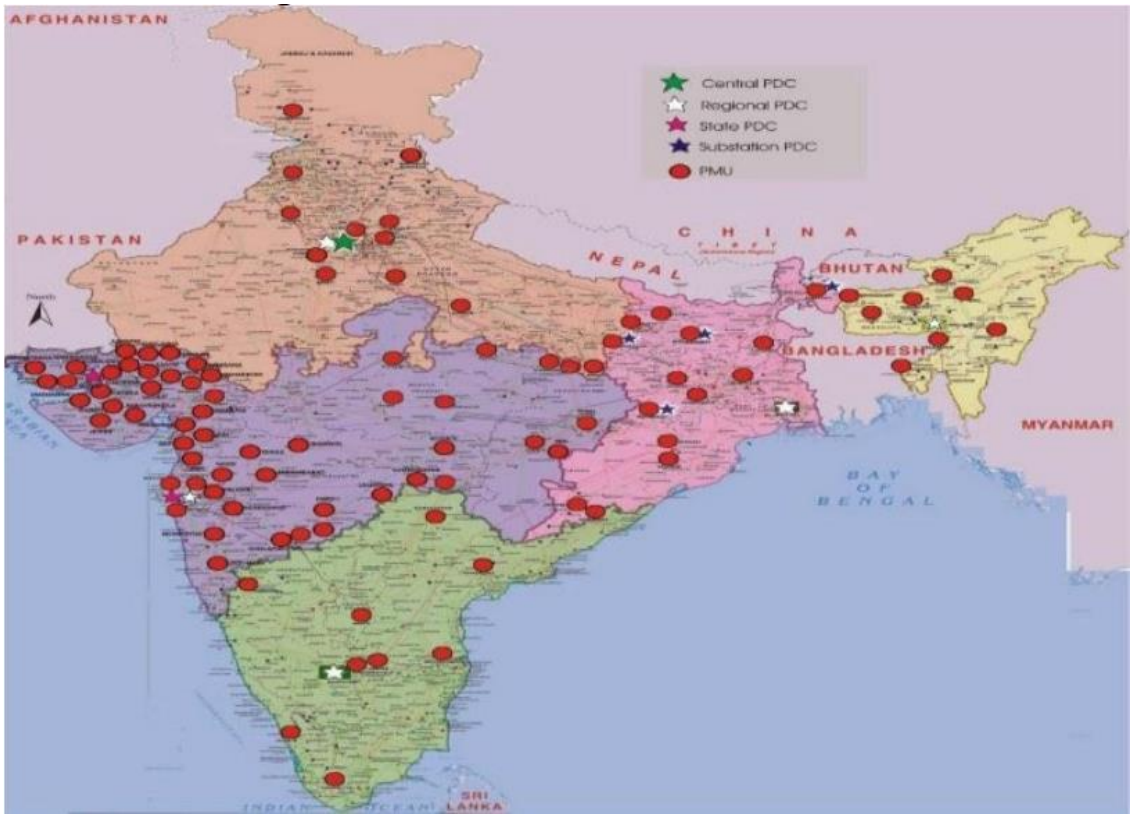

Figure 16- PMUs installed in India [40].

In Figure 16, the red dots represent PMUs, the green stars represent central PDCs, the white stars represent regional PDCs, the pink stars represent state PDCs, and the blue stars represent substation PDCs.

2.2.1.2 Optimal Placement Of PMU

As said earlier, PMU optimal placement aims for minimizing the installation cost of PMUs by finding the minimum number of PMUs in the network that gives full system observability and ensures the achievement of predetermined objectives and tasks [43], [44].

The optimal placement study can be done by numerical or topological observability.

Numerical observability relies on the Jacobian matrix of measurements being of

full rank [47]. Algorithms implementing this method need to build the Jacobian matrix for rank checking and this makes these algorithms more complicated [47].

In contrast, topological observability algorithms are more efficient because they rely on graph theory, meaning that the configuration of the power system and its connectivity reflect the necessary PMUs configuration and there is no need to build the full Jacobian matrix of measurements [47].

Using graph theory, if we consider a network graph G with *n* apexes (network buses) and *m* edges (network branches) the system is considered observable if there is a subgraph G' of G that contains all the apexes of G [44], [47].

Thus, by topological observability, the optimal placement problem is reduced to finding the minimal subgraph which contains all apexes of the network [44].

Using Ohm's and Kirchoff's circuit laws, topological observability implies that a bus connected to a PMU is directly observable and all buses connected to that bus are indirectly observable [44], [47], [48].

This is stated on the three rules of topological observability that follows:

1. Ohm's and Kirchoff's circuit laws determine that any bus can be observable if it is connected to a PMU bus [47].
2. By Ohm's law, any branch between two observed buses is observable [47].
3. If all incident branches are measured, Kirchoff's law can be used to estimate any branch current [47].

There are many algorithms for optimizing PMU placement, but if an algorithm focuses only on achieving full system observability the result may lead to unrealistic meter configuration as the power system probably already has a set of measurements installed [47]. The problem is that most algorithms proposed for optimal PMU placement doesn't take in consideration the existing measurement configuration of the power network before suggesting new schemes and the quality and numerical stability of the state estimation solution is compromised [47].

Another thing that impacts the stability of the state estimation solution is measurement redundancy. Although in case of meter failure, single power line outage and outages of multiple lines a higher local measurement redundancy being beneficial, it increases numerical instability of the state estimation solution and this represents a common drawback of many PMU placement techniques [47].

The top 25 articles regarding PMU optimal placement are reviewed in [47]. The

conclusion is that the majority of algorithms proposed, either based on numerical or topological observability, focus on optimizing PMUs configuration and treat measurement redundancy and bad data detection as an incremental feature and not a core feature of optimal PMU placement problem [47].

Optimal PMU placement techniques can be divided into two groups, the conventional and the non-conventional techniques [47].

The conventional techniques are linear programming, non-linear programming, dynamic programming, combinational optimization, and others. The non-conventional ones are particle swarm optimization, evolutionary algorithm, genetic algorithm, simulated annealing algorithm, and other search methods [47].

Figure 17 presents the taxonomy of optimization techniques for optimal PMU placement.

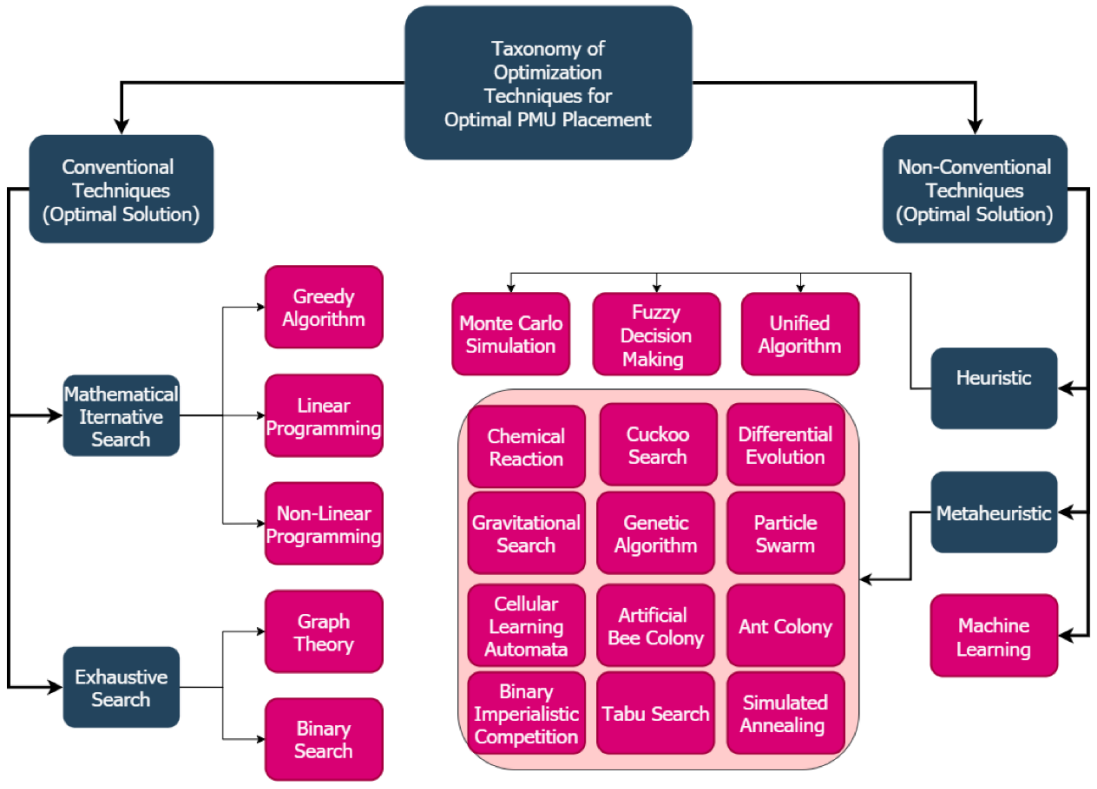

Figure 17- Optimization techniques used in optimal PMU placement [47].

In Figure 17, the techniques are divided into conventional and non-conventional and then grouped by methods. The conventional methods are based on mathematical iterative search and exhaustive search and the non-conventional are based on heuristic, metaheuristic, and machine learning.

Mathematical iterative algorithms use an initial value to make a sequence of improved estimates until the solution of two subsequent iterations converge to the same value up to three decimal places [47].

Exhaustive search algorithms require more time and computation power because they check every possible solution to the optimization problem, but these methods are recommended by [47] because they can run offline.

Heuristic techniques use a practical or shortcut method to give solutions that can or cannot be optimal in a limited timeframe [47].

Metaheuristic techniques guide through the search space to find near-optimal solutions ranging from local search to complex learning processes [47].

There are various machine learning algorithms that can be used for optimizing PMU placement, like fitting logistic regression models and training neural networks, but these methods rely on real-time data streaming to give optimal solutions [47].

Comparing the techniques, integer linear programming is better than other conventional techniques and metaheuristic, specifically particle swarm optimization and genetic algorithm, is better than heuristic and machine learning techniques [47].

2.2.1.3 Applications Of PMU

The PMU provides synchronized data with time that is useful for power system operation, protection, and control of the power system, having applications in state estimation, phasor-input security measures, phasor feedback for system control, the planning of corrective measures, measurement based control, adaptive protection, monitoring of stability and overloading and analysis of faults [36], [39], [40].

Furthermore, the usage of PMU has contributed to the creation of system models that allows quicker system restoration, post-disaster data processing and early warning systems and even made possible advances in state estimation architecture and algorithms [36].

Other applications of PMU data are computing Q-V and P-F curves of generators at different stages of load generation and the system arrangements [36].

2.2.1.4 PMU And State Estimation

Regarding state estimation, with the use of PMU it is possible to estimate the state of not completely observable networks. First you divide the system in observable and

unobservable islands, then do the state estimation of the observable portion and use the results to make close estimates of the unobservable parts of the network [39].

Figure 18 shows the use of PMUs in a partially observable network.

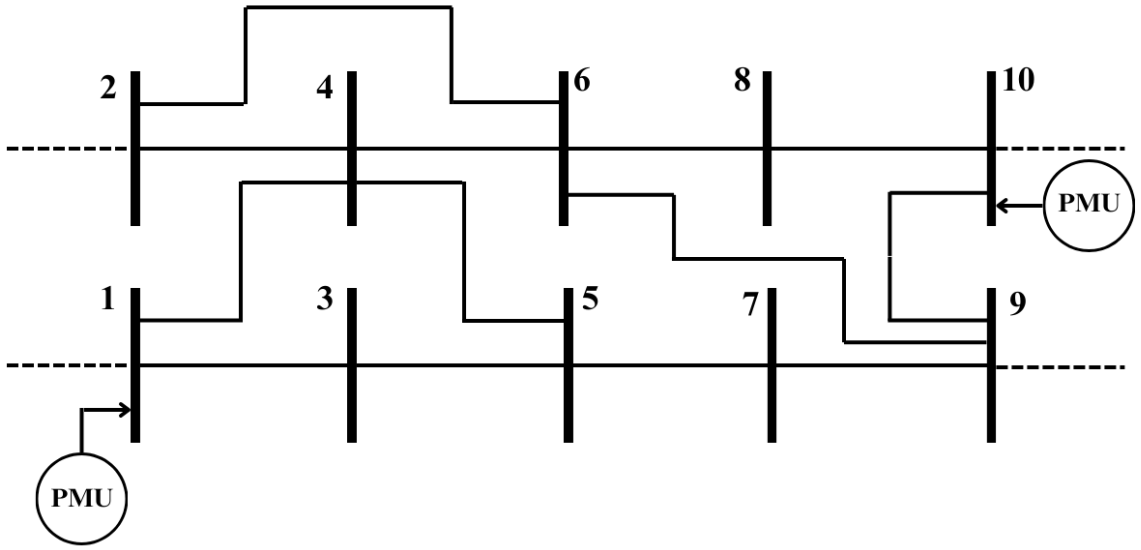

Figure 18- PMUs in a not completely observable network.

In Figure 18, two PMUs are placed on the network, turning part of it observable, but leaving some portions unobservable. Buses 1 and 10 are directly observed while buses 3, 4, 7, 8 and 9 are indirectly observed and buses 5 and 6 are not observed.

There are two ways to include phasor measurements of the PMU to state estimation [36], [39]. One of them is by combining the traditional P, Q measurements and phasor measurements to make a new hybrid non-linear state estimator and the other is by leaving intact the state estimator software and then using the phasor measurements in a linear post-processing step [39].

In general, the use of PMU data can make state estimation more efficient, accurate, robust and fast, provide direct observation of the state of the system and may even allow the implementation of estimators based on the least average value (LAV) method which were not the best option to use with SCADA measurements because LAV has problems with leverage measurements, but using PMU these leverage measurements can be eliminated [42], [44], [49].

2.2.1.5 PMUs And Power System Control

Regarding control, the synchronized data of the PMU makes it possible to use remote measurements when controlling power system stabilizers, excitation systems of

generators, HVDC terminals, and Flexible Alternating Current Transmission System (FACTS) devices [36], [39].

The use of these remote measurements are advantageous because the controllers don't rely on local measurements nor mathematical models of the larger system, which can provide bad results when inaccurate [39], [43].

Load shedding control can be improved by PMU synchronized measurements, making possible the construction of more flexible load shedding schemes [43].

2.2.1.6 PMUs And Power System Protection

Regarding protection, remote phasor measurements provided by PMU are used on adaptive relaying to prevent false trips of breakers and can also be used to identify risks of instability in the system that can lead to major system outages [36], [39], [43].

Moreover, various protection techniques can be used with PMU devices to pinpoint fault locations and restore electricity services [43], [49].

When there's loss of synchronism between areas of a power system or between interconnected power systems the areas must be separated in order to avoid equipment damage or shutdown of portions of the system [50]. PMU fast communication systems and phase angle measurements are advantageous to loss of synchronism protection and different schemes using PMU are studied [49].

2.2.1.7 PMU vs SCADA

PMU technology is the advanced version of SCADA [36] and a comparison is made in Table 1.

Table 1- Comparison between SCADA and PMU measurement systems [40].

Number	Parameter	SCADA	PMU
1	Type of measurement	Steady state measurement	Dynamic measurement
2	Level of monitoring	Local level monitoring	Wide area level monitoring
3	Measurement of phasor angle	Not possible	Possible

4	Resolution	Low	High
5	Time stamp	No	Yes
6	Post fault analysis	Not possible in real time	Possible in real time

As Table 1 shows, SCADA is limited to steady state measurement on a local level with low resolution and no time stamp and with it it's not possible to measure phasor angles nor make post fault analysis in real time. Meanwhile, PMU allows these options and provide dynamic measurements on a wide area level with high resolution and time stamp. Additionally, PMUs cost much more than SCADA.

Another significant difference between SCADA and PMU is noted on time steps for data collection. While SCADA time steps range from 4 seconds to 15 minutes, PMU time steps range from milliseconds to minutes [38].

On top of that, SCADA measurements aren't good enough to monitor varying effects in the system when it isn't in a stable condition due to its low sampling rate, slow detection of errors and time unsynchronized data [43]. All of these are solved with PMU.

2.2.2 Graph Theory

Currently, Graph Theory is one of the most important areas of discrete mathematics because it has applications in various fields and provides an ideal model for studying the relationships between discrete objects, whether it is a road map or a section of an electrical network.

Graphs are an abstract representation of relationships between objects, where objects are represented by vertices (or nodes), and relationships are represented by edges (or arcs) that connect the vertices [51]. Edges can be directed (the graphs are called directed graphs or digraphs) or undirected (the graphs are called undirected graphs).

They are commonly used to model a binary relationship between objects belonging to the same domain [52]. For example, vertices can represent electrical network buses, and edges can represent directly connected bus pairs. In the classic problem of the Königsberg bridges, vertices can represent parts of a city, and edges can represent the bridges connecting them. Alternatively, consider subway stations as vertices in a graph and subway lines as the edges.

Visual representation is often a way to facilitate the understanding of concepts,

problems, reasoning, and more. For example, it is more practical and quicker to create a graph of subway stations and lines in the previous example than to memorize which station has a connection with another and through which line. That's why graphical representation is commonly used for graphs, with points indicating vertices and lines representing edges, indicating the pairs of vertices that are connected [52].

Figure 19 displays the graphical representation of two graphs, each with five vertices and eight edges.

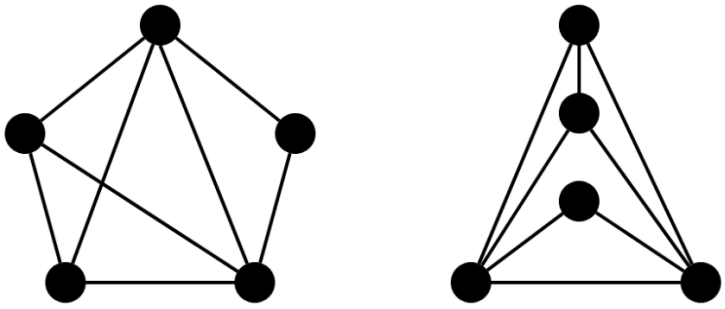

Figure 19- Graphical representation of two graphs with five vertices and eight edges [52].

2.2.2.1 Representing Graphs Through Matrices

A particularly important feature of graphs that makes them interesting for the study and analysis of power systems is their association with matrices. This association allows for the reflection of graph properties in the algebraic properties of matrices [52].

More specifically, symmetric matrices are crucial in this study due to adjacency matrices, incidence matrices, and Laplacian matrices, which are symmetric matrices. Through their spectral decomposition and the analysis of their eigenvalues and eigenvectors, important information about the graph can be obtained [52], [53].

The adjacency matrix of a graph is an integer matrix with rows and columns indexed according to the vertices of the graph [52]. It is a binary matrix, in the case of an unweighted graph, representing the connections between the vertices of the graph. If a pair of vertices is connected, it is assigned the number of connections; otherwise, it is assigned zero.

Figure 20 represents a graph from which the adjacency matrix will be assembled.

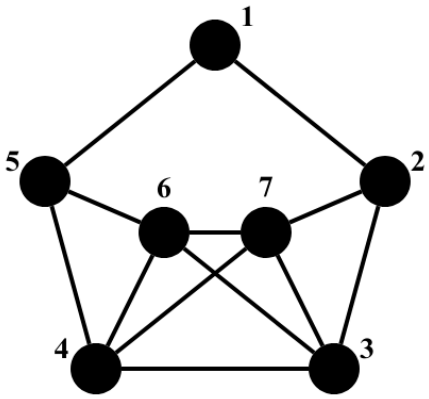

Figure 20- Example of a graph for assembling the adjacency matrix.

The above graph has seven vertices, so its adjacency matrix will be a 7x7 matrix:

$$\begin{bmatrix} 0 & 1 & 0 & 0 & 1 & 0 & 0 \\ 1 & 0 & 1 & 0 & 0 & 0 & 1 \\ 0 & 1 & 0 & 1 & 0 & 1 & 1 \\ 0 & 0 & 1 & 0 & 1 & 1 & 1 \\ 1 & 0 & 0 & 1 & 0 & 1 & 0 \\ 0 & 0 & 1 & 1 & 1 & 0 & 1 \\ 0 & 1 & 1 & 1 & 0 & 1 & 0 \end{bmatrix}$$

By this adjacency matrix, it is possible to determine which vertices are connected to others. However, another important aspect of the adjacency matrix is that its spectrum corresponds to the spectrum of the graph itself. Therefore, its eigenvalues and eigenvectors are treated as those of the graph [52].

Thus, each graph is also associated with a characteristic polynomial and its roots. In the case of the graph taken in the example, its characteristic polynomial is $(x+2)(x+1)^2(x-1)^2(x^2-2x-6)$ and its spectrum is {-2. -1, 1, $1 \pm \sqrt{7}$}, with roots 1 and -1 having multiplicity two. This spectrum is related to the number of vertices and edges in the graph.

The incidence matrix represents the connections between vertices and edges of the graph. It is not necessarily a binary matrix, and if *v* is the number of vertices and *a* is the number of edges, the incidence matrix is a *v* x *a* matrix.

Taking the graph from Figure 21 as an example to facilitate the understanding of constructing the incidence matrix:

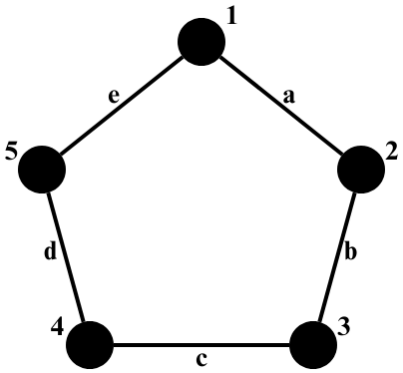

Figure 21- Example of a graph for constructing the incidence matrix.

The incidence matrix is:

$$\begin{array}{c} \\ 1 \\ 2 \\ 3 \\ 4 \\ 5 \end{array} \begin{array}{c} \begin{array}{ccccc} a & b & c & d & e \end{array} \\ \begin{bmatrix} 1 & 0 & 0 & 0 & 1 \\ 1 & 1 & 0 & 0 & 0 \\ 0 & 1 & 1 & 0 & 0 \\ 0 & 0 & 1 & 1 & 0 \\ 0 & 0 & 0 & 1 & 1 \end{bmatrix} \end{array}$$

In the case of a directed graph, meaning its edges have a direction, the incidence matrix reflects this orientation. The vertex from which the edge originates receives -1 in the matrix, and the vertex at which the edge terminates receives one.

Taking the graph from the previous example and adding direction to its edges in Figure 22

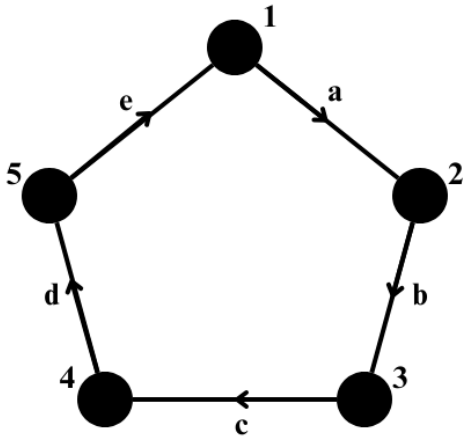

Figure 22- Example of an oriented graph.

The incidence matrix for this directed graph would be as follows:

$$\begin{array}{c} \\ 1 \\ 2 \\ 3 \\ 4 \\ 5 \end{array}\begin{array}{c} \begin{array}{ccccc} a & b & c & d & e \end{array} \\ \begin{bmatrix} -1 & 0 & 0 & 0 & 1 \\ 1 & -1 & 0 & 0 & 0 \\ 0 & 1 & -1 & 0 & 0 \\ 0 & 0 & 1 & -1 & 0 \\ 0 & 0 & 0 & 1 & -1 \end{bmatrix} \end{array}$$

Now, regarding the Laplacian matrix, this matrix is related to the structural properties of the graph and can provide important geometric representations of a graph. The Laplacian matrix has a special connection with the adjacency matrix because its eigenvectors are the same as those of the adjacency matrix, and its eigenvalues are determined by the eigenvalues of the adjacency matrix, but taking into account the graph's degree [52].

The degree of a vertex in a graph corresponds to the number of edges incident to that vertex. If all the vertices in the graph have the same degree, the graph is regular, and its degree is the same for all vertices [51].

Thus, if the adjacency matrix of a regular graph with degree k has eigenvalues $\theta_1, \dots, \theta_n$, the eigenvalues of the Laplacian matrix of this graph are $k - \theta_1, \dots, k - \theta_n$ [52].

The Laplacian matrix (L) can be constructed from a mathematical relationship between the degree matrix (D) and the adjacency matrix (A) [53].

$$L = D - A \tag{2.42}$$

The degree matrix is a diagonal matrix whose elements represent the degree of each vertex in the graph. So, the degree matrix for the graph in Figure 20 is

$$\begin{bmatrix} 2 & 0 & 0 & 0 & 0 & 0 & 0 \\ 0 & 3 & 0 & 0 & 0 & 0 & 0 \\ 0 & 0 & 4 & 0 & 0 & 0 & 0 \\ 0 & 0 & 0 & 4 & 0 & 0 & 0 \\ 0 & 0 & 0 & 0 & 3 & 0 & 0 \\ 0 & 0 & 0 & 0 & 0 & 4 & 0 \\ 0 & 0 & 0 & 0 & 0 & 0 & 4 \end{bmatrix}$$

And now, calculating its Laplacian matrix:

$$L = \begin{bmatrix} 2 & 0 & 0 & 0 & 0 & 0 & 0 \\ 0 & 3 & 0 & 0 & 0 & 0 & 0 \\ 0 & 0 & 4 & 0 & 0 & 0 & 0 \\ 0 & 0 & 0 & 4 & 0 & 0 & 0 \\ 0 & 0 & 0 & 0 & 3 & 0 & 0 \\ 0 & 0 & 0 & 0 & 0 & 4 & 0 \\ 0 & 0 & 0 & 0 & 0 & 0 & 4 \end{bmatrix} - \begin{bmatrix} 0 & 1 & 0 & 0 & 1 & 0 & 0 \\ 1 & 0 & 1 & 0 & 0 & 0 & 1 \\ 0 & 1 & 0 & 1 & 0 & 1 & 1 \\ 0 & 0 & 1 & 0 & 1 & 1 & 1 \\ 1 & 0 & 0 & 1 & 0 & 1 & 0 \\ 0 & 0 & 1 & 1 & 1 & 0 & 1 \\ 0 & 1 & 1 & 1 & 0 & 1 & 0 \end{bmatrix} = \begin{bmatrix} 2 & -1 & 0 & 0 & -1 & 0 & 0 \\ -1 & 3 & -1 & 0 & 0 & 0 & -1 \\ 0 & -1 & 4 & -1 & 0 & -1 & -1 \\ 0 & 0 & -1 & 4 & -1 & -1 & -1 \\ -1 & 0 & 0 & -1 & 3 & -1 & 0 \\ 0 & 0 & -1- & -1 & -1 & 4 & -1 \\ 0 & -1 & -1 & -1 & 0 & -1 & 4 \end{bmatrix}$$

(2.43)

The study of the eigenvalues and eigenvectors of a graph's Laplacian matrix give valuable information about the connectivity of the graph and the power system it represents. Algorithms for state estimation and parameter identification based on graph theory manipulate the Laplacian matrix as the eigenvalues contain crucial details regarding the flow of current within an electrical network and the eigenvectors represent the boundary voltage values where the boundary voltage equals a scalar multiple of the boundary current [54].

2.2.2.2 Particular Families Of Graphs And Major Definitions

Graphs can be divided into smaller structures called subgraphs. These subgraphs contain only a specific set of vertices and edges from the original graph. This allows for the analysis or study of specific parts of a larger graph, identifying local patterns or properties. Applying this to the power system, one could study specific portions of a large electrical network, for example.

Additionally, graphs are classified into specific groups called families due to some common characteristics. Some of the major graph families and definitions are [51], [52]:

- Regular graphs – graphs where every vertex has the same degree.
- Bipartite graphs – graphs whose vertices can be divided into two independent sets such that every edge connects a vertex from one set to the other.
- Complete graphs - graphs in which each pair of vertices is connected by an edge.
- Complete bipartite graphs – special kind of bipartite graphs in which each pair of vertices is connected by an edge.
- Connected graphs – graphs where for each pair of vertices, there exists at least one single path which joins them. All complete graphs are connected graphs, but not all connected graphs are complete graphs as in a connected graph it may take more than one edge to get from one vertex to another.
- Cyclic graphs – graphs in which is possible to form at least one closed path where the first and last vertices are equal.
- Tree – undirected graphs in which any two vertices are connected by one unique path.

- Forest - undirected graphs where any pair of vertices is linked by a maximum of one path, in other words, a disjoint union of trees.
- Spanning tree of a graph - a subset of a connected undirected graph that covers all vertices with the fewest edges needed.
- Clique of a graph - a group of vertices in an undirected graph where every pair of distinct vertices in the group are connected.
- Maximal clique of a graph - a clique that cannot be expanded by adding another adjacent vertex, meaning it does not exist solely within the vertex set of a larger clique.

Knowing this major definitions and families of graphs is crucial to applying the theory to state estimation, topology analysis, observability analysis and parameter identification. However, more classifications and families of graphs are defined in the literature [51], [52].

2.2.3 State Estimation

State estimation is a technique that aims to determine the most likely state of the power system at a given moment based on measurements of some of the system's quantities, such as generator output powers, line currents, and bus voltages [27].

The study of this technique began in the 1970s, but it only gained more prominence in the 1990s when it started to play a significant role in power system operation [27], [55], [56]. Today, it is a fundamental component for control centers, especially with the increasing complexity resulting from the uncertainties by the new technologies being deployed in the generation and demand sides [27], [56], [57].

The identification of the operational state ensures the system operates safely and outlines necessary actions for maintaining this state, however, for this, constant monitoring of the system is necessary [27].

Among the typical measurements are power flow on transmission lines, magnitudes of bus voltages, currents in lines, generator powers, loads, information about circuit breakers and their states, tap positions of transformers, and values of switchable capacitor banks [27], [55].

These measurements used to be provided by SCADA systems and relied on the steady-state model of the power grid but due to stochastic changes in demand and generation aggravated by the large-scale integration of DERs, complex loads and new

demand-response technologies the steady-state assumption is questionable and more dynamic measurement systems are needed [27], [55], [56], [57]. Currently, PMU measurements are being used to perform dynamic state estimation and this provides some benefits like improved oscillations monitoring, enhanced hierarchical decentralized control, improved dependability and reliability of protection systems, enhanced reliability of system models and more [55], [57].

This state estimator filters measurement data, detects errors, and provides a database for various applications such as contingency analysis, automatic generation control, load forecasting, and optimal power flow [27]. They typically include the following functions [27], [58]:

- Topology Processor – gathers data from breakers and switches and assembles the one-line diagram of the system.
- Observability Analysis – determines if the state estimation of the entire system is possible from a set of data and identifies unobservable branches and observable islands, if any.
- State Estimation Solution – determines the optimal estimate of the system state, which consists of the complex voltages of all buses, based on the network model, and obtained measurements. It also provides the best estimates for line flows, loads, transformer tap settings, and generator power.
- Invalid Data Detection – detects errors in received measurements and eliminates them if the measurement configuration provides sufficient redundancy.
- Structural and Parameter Error Processing – estimates various parameters of the network, such as transmission line models, transformer tap parameters, and parameters of shunt reactance or capacitance. It also detects errors in the network configuration and identifies circuit breaker state errors if there is redundancy in the measurements.

Figure 23 presents a flowchart of power system security analysis using state estimation.

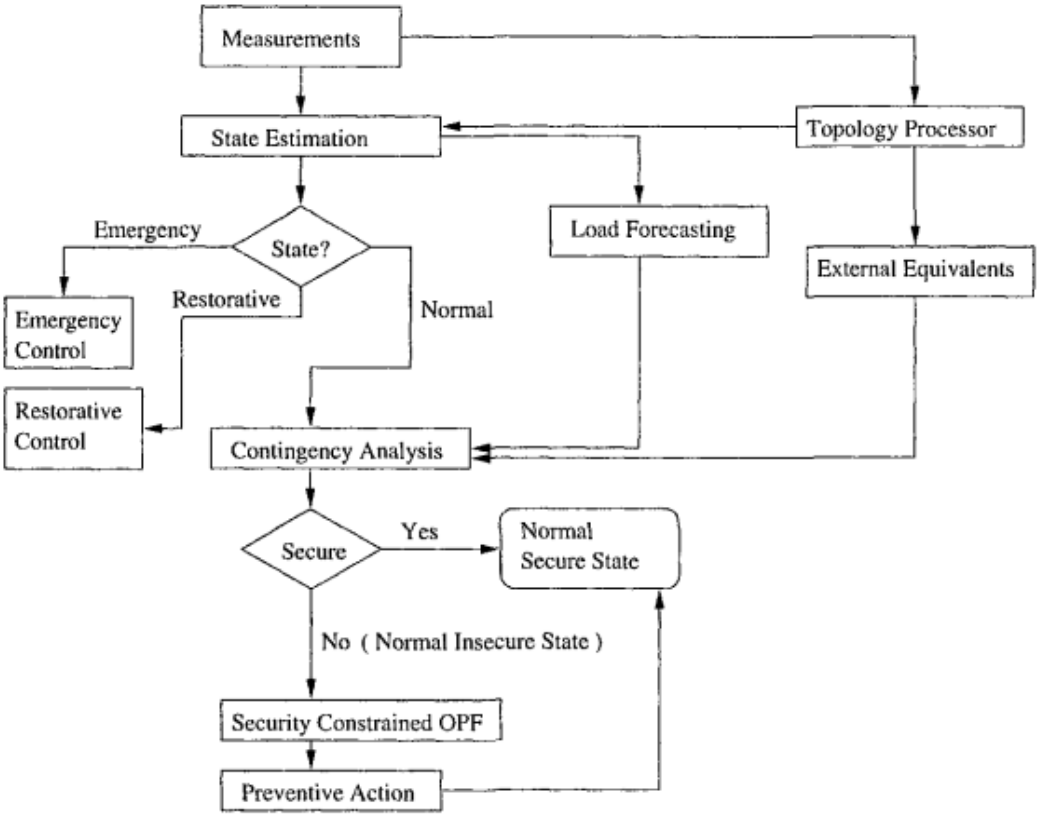

Figure 23 - Flowchart of power system security analysis with state estimation [27].

According to Figure 23, the network's topology is constructed from measurements, and state estimation is performed. The current system state is obtained from the state estimation solution, and necessary actions are taken. If the state is in an emergency, emergency control is initiated. If the state is restorative, restorative control is initiated. If the operating state is normal, contingency analysis is conducted, and if necessary, preventive action is taken to maintain the system in a safe normal operating state.

The most used algorithms to solve state estimation are based on the maximum likelihood estimation (MLE) and weighted least squares (WLS) methods [27], [56], [59].

In MLE, it is assumed that measurement errors follow a normal Gaussian distribution with unknown mean and variance, and each measurement has a probability density function (PDF) [27], [57]. The combination of the PDFs of all measurements generates a function called the likelihood function, which must be maximized with respect to the means and variances of the measurement errors to obtain the maximum likelihood for the desired parameters [27], [57]. The maximization of the likelihood function is done

using a weighted least squares method algorithm [27].

2.2.3.1 State Estimation Techniques

The efficiency of state estimation techniques varies with the type of operating condition of the power system. A transient state occurs when sudden eletromechanical disturbances takes places on the system and a quasi-steady state occurs when the changes in the system happen slowly and smoothly and due exclusively to load and renewable generation changes [55], [57].

State estimation techniques can use conventional measurements when the system is in a quasi-steady state but during transient states the state estimation may only be performed when synchrophasor measurements are available [57], [60].

Some of the techniques of state estimation are [56], [57], [61]:

- Dynamic state estimation (DSE) – this technique usually consists of a parameter prediction step and a filtering step developed within a nonlinear Kalman filter. However, some dynamic estimators are constructed using other types of filters such as infinite impulse response filter and finite impulse response filter. This technique can be used virtually in all power systems but when applied to a quasi-steady state operating condition it is usually referred to as forecasting-aided state estimation or tracking state estimation.
- Forecasting-aided state estimation (FASE) – a particular application of DSE to quasi-steady state conditions in which state-transition model is assumed to be linear. On this technique, values are calculated based on a weighted average of recent past values, utilizing exponentially decreasing weights and without consideration of other information about the specific problem structure. If applied in systems with fast scanning rates, it provides useful information for security analysis and preventive control functions.
- Tracking state estimation (TSE) – a simplified version of the previous method that assumes a quasi-steady state condition where the system's state is represented by a white Gaussian noise. With this technique, modeling the power system's dynamics cannot be made appropriately and because of this it is a challenge to use it in practical applications.

- Static state estimation (SSE) – a further simplification of tracking state estimation that ignores state transition information and has no memory of the states at previous time steps. It responds better than FASE and TSE to sudden changes in the power system but cannot track system dynamics like DSE.
- Linear state estimation (LSE) – a variation of SSE able to track phasors in real time at PMU reporting rate but is not able to track system dynamics.

A performance comparison of state estimation techniques is done in [62] and more in depth explanations of these techniques are done in [56], [57], [58].

2.2.3.2 Observability Analysis For State Estimation

A power system is said to be observable if the measurements made on it allow determining the magnitude and phase angle of voltages at all busbars in the network [63], [64].

The analysis of a set of measurements and their locations can determine if the system is observable and if state estimation is feasible [27], [57]. If the entire system is not observable, state estimation is not possible, or it is possible only for some observable sections of the system. In that case, the installation of meters at specific locations in the power system is required [27].

Telecommunication errors, changes in the power system's topology, or meter failures may result in state estimation being possible only for observable islands that are isolated from each other, each island having its own reference angles for the voltages and currents at the buses [27]. Because of this, the observability of a power network is seen as time dependent [57].

Observability analysis methods can be classified into topological, numerical and hybrid methods [65]. Numerical analysis utilizes linear or nonlinear mathematical models and floating-point calculations to determine if the system is fully or partially observable [27], [57]. This numerical study can be computationally heavy and the attempt to simplify it often leads to incorrect results under highly nonlinear operating conditions [57]. Meanwhile, topological analysis ties the power system's equations and solutions to graphs, making the algorithms computationally advantageous because they only rely on logical operations, however requires information about network connectivity, the type of measurement, and its location [27]. Hybrid methods, on the other hand, use the

topological methods to simplify the network scale before conducting the numerical observability analysis [65].

In topological observability analysis, power flow measurements are assigned to the corresponding edges of the electrical network graph, attempting to form a spanning tree of this graph. If it is not possible to form the spanning tree, a forest containing small trees of the graph is formed, and power injection measurements are used to try to connect these small trees and form a single tree, classifying the system as observable [27], [65].

Thus, it is said that if a tree can be formed in the graph of the network where each branch has a power flow measurement, then the phase angles at all buses can be determined, and the system is fully observable.

However, if it is not possible to form a spanning tree after assigning power flows and injections, the observable islands of the system must be identified [27]. This process is conducted in two steps:

1. Discard the power injections related to a bus that has at least one incident branch that does not form a loop with the branches of the forest defined during topological analysis.
2. Update the forest according to the discarded injections and repeat step 1 until there are no more injections to be discarded.

For a better understanding, a topological analysis will be performed on the system shown in Figure 24.

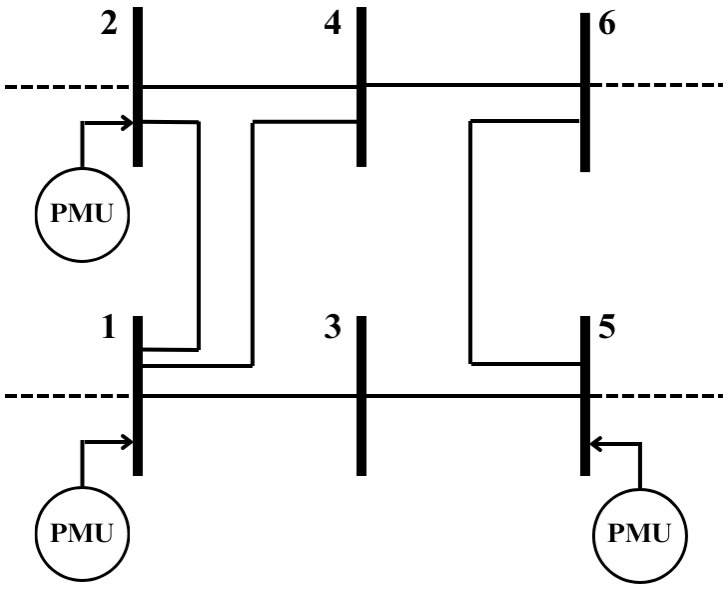

Figure 24- Power system for topological analysis example.

In Figure 24 the electrical system consisting of six buses has power injection measurements at buses 1, 2, and 5 and does not have power flow measurements. The graph representing this electrical network is shown in Figure 25.

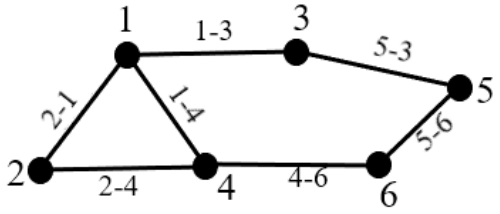

Figure 25 - Graph of the electrical network for the topological analysis example.

Following step 1 of the algorithm, one should assign the power flow measurements to the lines for the graph formation. However, as there are no available power flow measurements in the presented system, we proceed to step 2.

In step 2, the power injections at buses 1, 2, and 5 are assigned to one of the branches connected to these buses, arbitrarily. The injection at bus 1 is assigned to branch 1-3, the branch between buses 1 and 3. The injection at bus 2 is assigned to branch 2-1, and the injection at bus 5 is assigned to branch 5-3.

The formed forest is presented in Figure 26.

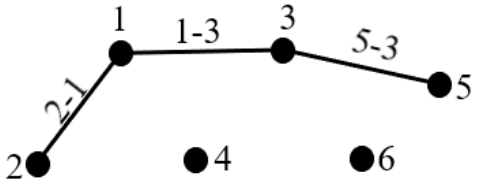

Figure 26 - Graph formed after assigning available power injections.

As shown in Figure 26, after processing the power flows and injections, a spanning tree of the system graph was not found, as vertices 4 and 6 remained isolated. It is then concluded that the entire system is not observable, and we proceed to the analysis of observable islands.

In step 3, we must analyze buses 1, 2, and 5 and check if they are associated with branches that do not form a loop with the forest presented in Figure 26. Analyzing bus 1, it is associated with branches 1-3, 2-1, and 1-4. Branches 1-3 and 2-1 are present in the forest defined in Figure 26, but branch 1-4 is not. If included in the forest, it would not form a loop, as shown in Figure 27.

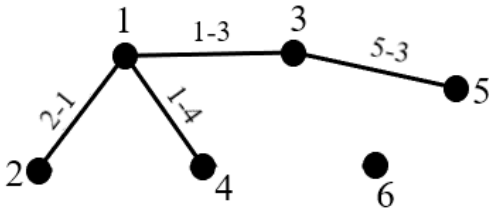

Figure 27- Branch 1-4 not forming a loop in the defined forest.

Therefore, the power injection at bus 1 should be discarded, and the forest from Figure 26 should be updated by removing the branch 1-3, a branch that was attributed due to injection 1. The updated forest is presented in Figure 28.

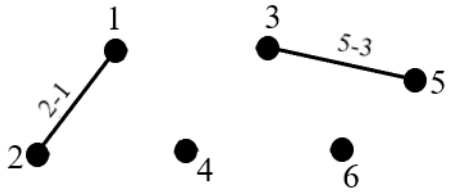

Figure 28- Updated forest after removal of injection 1.

Now analyzing bus 2, it is associated with branches 2-1 and 2-4. Branch 2-1 is present in the forest, but branch 2-4 is not, and if added to the forest, it would not form a loop, as shown in Figure 29.

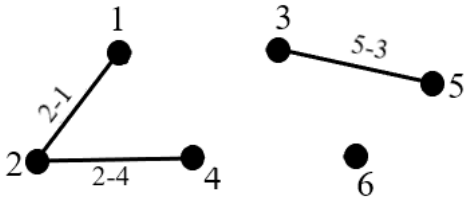

Figure 29- Branch 2-4 not forming a loop with the updated forest.

Therefore, injection 2 should also be discarded, and the updated forest is shown in Figure 30.

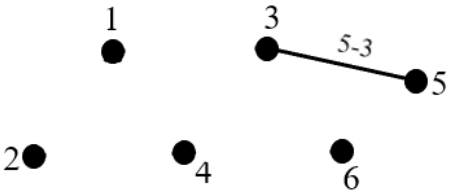

Figure 30- Updated forest after removal of injection 2.

Finally, analyzing bus 5, it is associated with branches 5-3 and 5-6. Branch 5-3 is present in the forest, but branch 5-6 is not, and it would not form a loop in the forest. Therefore, the injection at bus 5 is also discarded. The updated forest is shown in Figure 31.

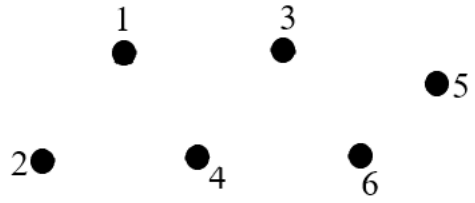

Figure 31- Updated forest after discarding all power injection measurements.

This way, all power injections in the system were discarded, and the system, besides not being entirely observable, does not have observable islands.

The algorithm developed in [57] presents a generic method based on the main steps to perform topological analysis, but more detailed algorithms can be found in [63], [66], for example.

2.3 Synthesis

In traditional methods, transmission line parameters are derived from the line conductors' geometry and length or measured directly using specific instruments during transmission line construction or maintenance. However, these approaches are often inaccurate due to simplified models or impractical since they can only be applied when the line is offline.

Modern techniques enable the estimation of line parameters by applying Kirchhoff's and Ohm's laws to solve nonlinear equations derived from the equivalent π model of the transmission line. This is achieved using PMU measurements of voltage and current phasors, employing methods such as WLS, state estimation, residual sensitivity analysis, and WLS-based augmented state estimation.

While these modern techniques offer advantages over classical methods, their accuracy relies not only on convergence but also on the precision of phasor measurements and state estimation. For example, PMUs synchronized via GPS transmit measurements to the control center with a time stamp to match measurements at both ends of a line. However, some measurements may be missing, and uncertainties can arise from the instrument transformers' low accuracy class. Additionally, interference and signal

distortions in the measurement process can further compromise data accuracy.

3. Methodology

Two techniques are proposed to estimate transmission line parameters.

The first one applies Kirchhoff's law to derive equations from the equivalent π model of the transmission line to find the line parameters from current and voltage phasors. This methodology will often be referred to as methodology one or first methodology.

The second one exploits a set of current and voltage phasors to identify the admittance matrix of the system by solving an optimization problem and then retrieving the line parameters and is based on the work presented in [10]. This methodology will often be referred to as methodology two or second methodology.

These methodologies are explained in the following subtopics.

3.1 Kirchhoff's Law Based Line Parameter Estimation

In this methodology, the nominal π model of a transmission line is utilized to determine the lumped values of the line's series resistance, reactance, and shunt susceptance based on voltage and current phasor measurements provided by PMUs installed at both ends of the line on a time basis.

The nominal π model was presented in the topic 2.1.1.2 along with the equations of voltage and current associated with this model. A simple mathematical manipulation on those equations makes possible to express the lumped series impedance and shunt admittance of the line in terms of the receiving and sending ends currents and voltages.

However, with the inverse power flow introduced by renewable energies in the power system, consider the nominal π model of Figure 32.

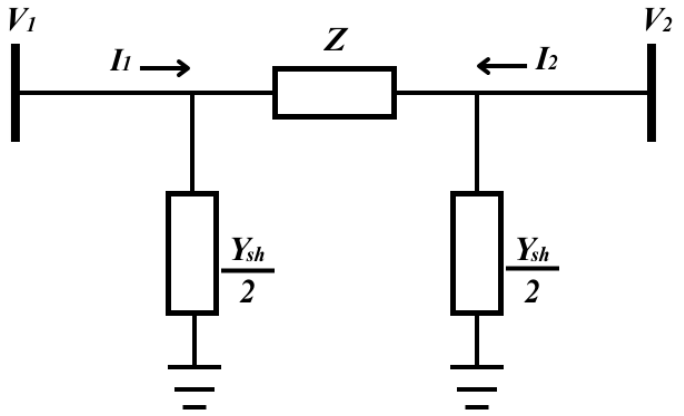

Figure 32 – Nominal π model with inverse power flow represented.

The equations derived for this circuit are remarkably like those derived for the nominal π model and thus will not be shown. Expressing the lumped series impedance and the shunt admittance in terms of the currents and voltages and the circuits give us

$$Z = \frac{(V_1 - V_2)(V_1 + V_2)}{I_1(V_1 + V_2) - V_1(I_1 + I_2)} \tag{3.1}$$

$$\frac{Y_{sh}}{2} = \frac{I_1 + I_2}{V_1 + V_2} \tag{3.2}$$

Lumped series resistance and reactance are then obtained by taking the real and imaginary parts of the calculated impedance, respectively.

The shunt conductance and susceptance are obtained by taking the real and imaginary parts of the calculated shunt admittance.

3.2 Line Parameter Estimation Based On Admittance Matrix Identification

The difference from the previous methodology to this one is that on this there are multiple measurements available for every bus of the grid and all these measurements are used to construct the vectorial form of the Kirchhoff's law.

Based on the vectorial form of the Kirchhoff's law an optimization problem is formulated and solved to obtain the admittance matrix of the network and then from the admittance matrix the line parameters can be retrieved.

Consider a power system composed of N buses, each having K voltage and current phasorial measurements available. For a given bus i of the N buses of the network, the vectorial form of Kirchhoff's law is

$$\underbrace{\begin{bmatrix} I_i(1) \\ I_i(2) \\ \vdots \\ I_i(K) \end{bmatrix}}_{I_i(K)} = \underbrace{\begin{bmatrix} V_1(1) & V_2(1) & \cdots & V_N(1) \\ V_1(2) & V_2(2) & \cdots & V_N(2) \\ \vdots & \vdots & \ddots & \vdots \\ V_1(K) & V_2(K) & \cdots & V_N(K) \end{bmatrix}}_{V(K)} \underbrace{\begin{bmatrix} Y_{i1} \\ Y_{i2} \\ \vdots \\ Y_{iN} \end{bmatrix}}_{Y_i} \tag{3.3}$$

where $I_i(K)$ is the column vector of K current measurements of bus i, $V(K)$ is the matrix containing the K voltage measurements of all N buses of the network and Y_i is the column vector of the admittances between bus i and the other buses of the grid.

The admittance matrix can be obtained by solving the optimization problem formulated in [10]

$$\begin{aligned} &\hat{Y}^{K,l_2} \triangleq \arg\min_{Y} \left\| V(K)Y - I(K) \right\|_F \\ &s.t.: Y \in S^N, Y_{ii} = -\sum_{j \neq i} Y_{ij} \qquad \forall i = 1...N \end{aligned} \tag{3.4}$$

where the estimated admittance matrix $\hat{Y}^{K,l_2}$ is defined as the minimized admittance matrix Y, S^N is the set of all $N \times N$ complex symmetric matrices, meaning that Y is a symmetric but not Hermitian complex matrix, $I(K)$ is a $K \times N$ matrix representing the K current measurements of all N buses of the network, as

$$I(K) = \begin{bmatrix} I_1(K) & I_2(K) & \cdots & I_N(K) \end{bmatrix} \tag{3.5}$$

This constrained optimization problem can be converted to an unconstrained one and simplified to a quadratic problem in the real domain. For that reason, first consider that vectorized form of the full admittance matrix of the network $vec(Y)$ as

$$vec(Y) = \begin{bmatrix} Y_{11} & Y_{21} & \ldots & Y_{N1} & Y_{12} & Y_{22} & \ldots & Y_{NN} \end{bmatrix}^T \tag{3.6}$$

Then vectorizing the optimization problem

$$\begin{aligned} &\min_{vec(Y) \in \mathbb{C}^{N^2 \times 1}} \left\| \left(\mathrm{I} \otimes V(K) \right) vec(Y) - vec\left(I(K) \right) \right\|_2 \\ &s.t.: Y \in S^N, Y_{ii} = -\sum_{j \neq i} Y_{ij} \qquad \forall i \end{aligned} \tag{3.7}$$

where $\otimes$ is the Kronecker product and I is an $N \times N$ identity matrix.

Now, let $svec: S^N \to \mathbb{C}^{\left(N^2 - N\right)/2 \times 1}$ be a mapping from a symmetric complex matrix to a complex vector defined as

$$svec(Y) = \begin{bmatrix} Y_{21} & Y_{31} & \ldots & Y_{N1} & Y_{32} & Y_{42} & \ldots & Y_{NN-1} \end{bmatrix}^T \tag{3.8}$$

And based on this, $vec(Y) = \Gamma svec(Y)$ where $\Gamma \in \mathbb{R}^{N^2 \times (N^2-N)/2}$ is an operator that maps $svec(Y)$ to the vectorized admittance matrix. To exemplify this, consider the network show in Figure 33.

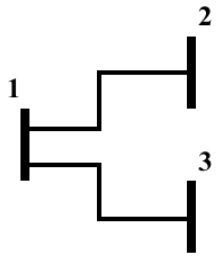

Figure 33- Three bus network example.

For this network, the relation between Γ, $vec(Y)$ and $svec(Y)$ is

$$\underbrace{\begin{bmatrix} Y_{11} \\ Y_{21} \\ Y_{31} \\ Y_{12} \\ Y_{22} \\ Y_{32} \\ Y_{13} \\ Y_{23} \\ Y_{33} \end{bmatrix}}_{vec(Y)} = \underbrace{\begin{bmatrix} -1 & -1 & 0 \\ 1 & 0 & 0 \\ 0 & 1 & 0 \\ 1 & 0 & 0 \\ -1 & 0 & -1 \\ 0 & 0 & 1 \\ 0 & 1 & 0 \\ 0 & 0 & 1 \\ 0 & -1 & -1 \end{bmatrix}}_{\Gamma} \underbrace{\begin{bmatrix} Y_{21} \\ Y_{31} \\ Y_{32} \end{bmatrix}}_{svec(Y)} \tag{3.9}$$

It is noteworthy that this definition of Γ and $svec(Y)$ are for and admittance matrix without shunt elements. But to redefine these terms to consider shunt elements is simple, $svec(Y)$ should include diagonal elements and Γ is updated accordingly.

Continuing, now updating the optimization problem with Γ

$$\min_{svec(Y) \in \mathbb{C}^{(N^2-N)/2 \times 1}} \left\| \left(\mathrm{I} \otimes V(K) \right) \Gamma svec(Y) - vec\left(I(K) \right) \right\|_2 \tag{3.10}$$

Considering $F \triangleq \left(\mathrm{I} \otimes V(K) \right) \Gamma$ and defining

$$\tilde{F} = \begin{bmatrix} \mathrm{Re}(F) & -\mathrm{Im}(F) \\ \mathrm{Im}(F) & \mathrm{Re}(F) \end{bmatrix} \tag{3.11}$$

and

$$\tilde{b} = \begin{bmatrix} \mathrm{Re}\left(vec\left(I\left(K\right)\right)\right) \\ \mathrm{Im}\left(vec\left(I\left(K\right)\right)\right) \end{bmatrix} \tag{3.12}$$

the optimization problem can now be written as an unconstrained quadratic problem in the real domain

$$\min_{\tilde{f}(Y)\in\mathbb{R}^{\left(N^2-N\right)\times 1}} \left\| \tilde{F}\,\tilde{f}\left(Y\right) - \tilde{b} \right\|_2 \tag{3.13}$$

where $\tilde{f}\left(Y\right) \triangleq \left[svec\left(\mathrm{Re}\left(Y\right)\right)^T \quad svec\left(\mathrm{Im}\left(Y\right)\right)^T \right]^T$ and $\mathrm{Re}\left(Y\right)$ is the real part of the minimized admittance matrix and $\mathrm{Im}\left(Y\right)$ is the imaginary part.

Finally, provided that $V\left(K\right)$ has full column rank, the least square problem solution is given by

$$\tilde{f}\left(Y\right) = \left(\tilde{F}^T \tilde{F} \right)^{-1} \tilde{F}^T \tilde{b} \tag{3.14}$$

From this, the admittance matrix of the network can be obtained in vectorized form by the relation $vec\left(Y\right) = \Gamma svec\left(Y\right)$ shown previously and then the line parameters can be retrieved from the elements of the vectorized admittance matrix.

4. Case Studies

Two case studies are developed on this work, one considering a five buses radial network and one considering the IEEE 14-bus test case system.

The case study considering the five buses radial network tests the proposed Kirchhoff's law based line parameter estimation method.

The case study using the IEEE 14-bus test case system tests both the Kirchhoff's law method and the method based on admittance matrix identification.

The case studies are presented in the following subtopics.

4.1 Five Buses Radial Network Case Study

This case study uses the radial power system with five buses, four transmission lines, two generators and three loads shown in Figure 34.

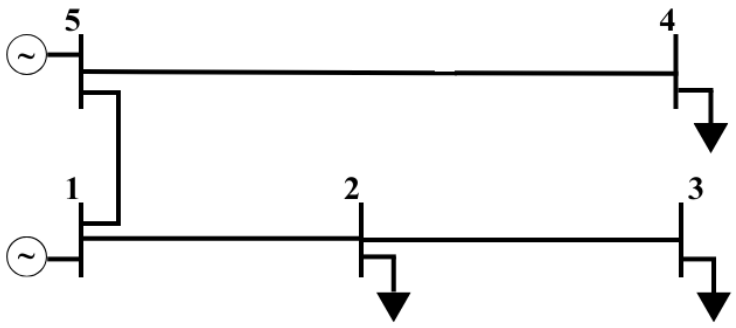

Figure 34- Five buses radial network test system.

The system has a base power of 100 MVA and base voltage of 230 kV. Bus 1 is the slack bus, bus 5 is a PV bus and buses 2, 3 and 4 are PQ buses.

Characteristics of the system like terminal conditions, line parameters and load characteristics are presented in the next tables.

Table 2 presents the terminal conditions of the system.

Table 2 – Terminal conditions of the radial system.

Bus	V (pu)	Θ (degrees)	P (MW)	Q (Mvar)
1	1	0	123,02	405,43
2	0,89	-10,45	0	0
3	0,88	-12,71	0	0
4	0,94	-5,21	0	0
5	1	1,83	900	147,6

Table 3 shows the line parameters in per unit for each line of the radial system.

Table 3 – Line parameters for the radial system.

Line	R (pu)	X (pu)	B (pu)
1-2	0,00281	0,0281	0,00712
1-5	0,00064	0,0064	0,03126
2-3	0,00108	0,0108	0,01852
4-5	0,00297	0,0297	0,00674

Table 4 presents the load characteristics for the radial system presented in Figure

34.

Table 4- Load characteristics for the radial system.

Bus	P (MW)	Q (Mvar)
2	300	98,61
3	300	98,61
4	400	131,47

The case study is constructed by twenty-four scenarios, each scenario simulating one hour of the day. The load demand and configuration are changed throughout these scenarios to simulate the changes that occur in a real power system.

To simulate the phasors measurements a series of power flows were conducted using Matpower, a package of open-source Matlab-language M-files designed for solving steady-state power system simulations [67]. The Newton method was employed for each case to determine the bus voltages and line current values required for estimating the line parameters. It is noteworthy that an error of $\pm 1\%$ is considered for the voltage magnitude values, simulating measurement errors.

Figure 35 presents the total active power generated and total active power consumed curves in each scenario.

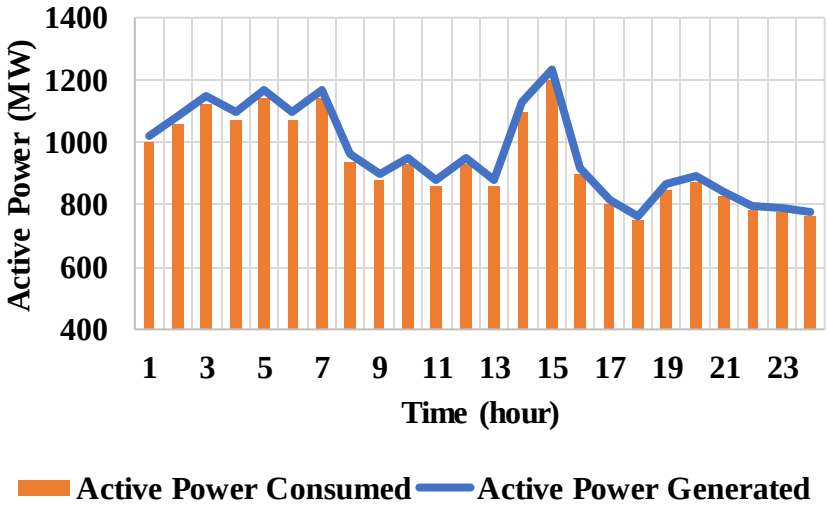

Figure 35- Total active power generated vs total active power consumed.

4.2 Fourteen Buses IEEE Meshed Network Case Study

The IEEE 14-bus network has fourteen buses, five generators and eleven loads

and is presented in Figure 36.

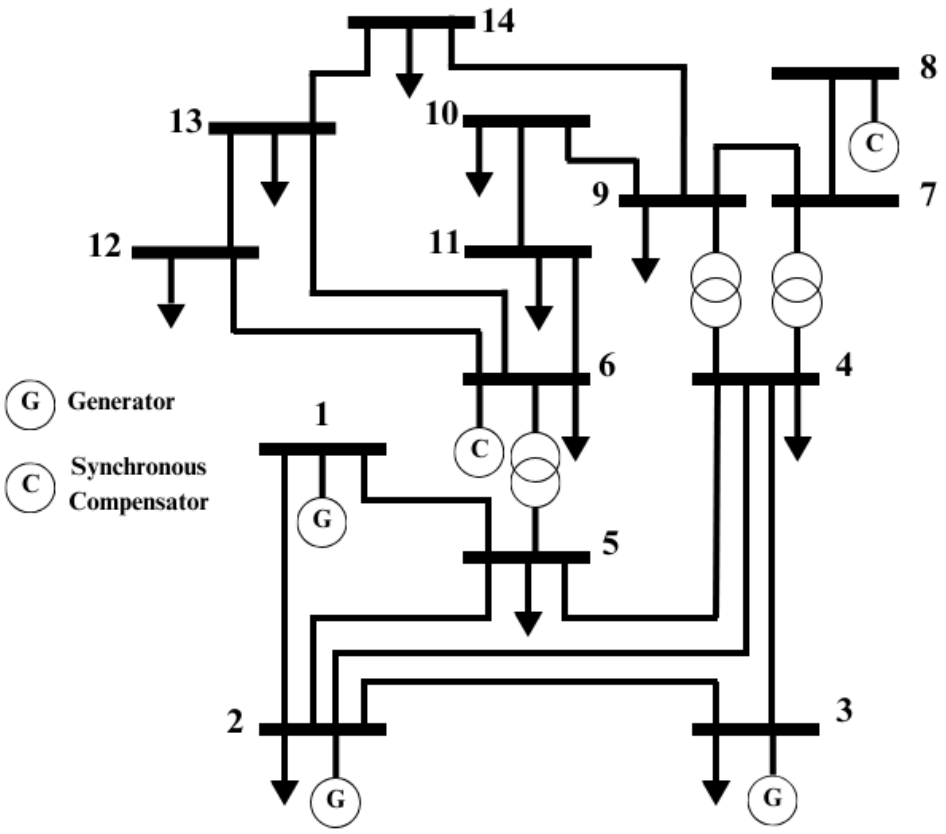

Figure 36 – IEEE 14-bus system.

In Figure 36, bus 1 is the slack bus, buses 2, 3, 6 and 8 are PV buses and the remaining are PQ buses.

Generators 1, 2 and 3 are modelled as voltage sources and generators 6 and 8 act like synchronous compensators.

Like the previous case study, a time series with one hour resolution, totaling 24 hours, is constructed for the loads and generators, aiming to simulate the behavior of the system in a day. The phasor measurements were also simulated like the previous case.

The loads considered in the time series are based on a mixed dataset of hourly load profiles [68], scaled accordingly to better fit the original system data given in [69].

The nominal system values considered are based on the ones presented in [69] and can be verified in Annex A.

The total active load and power generated are presented in Figure 37.

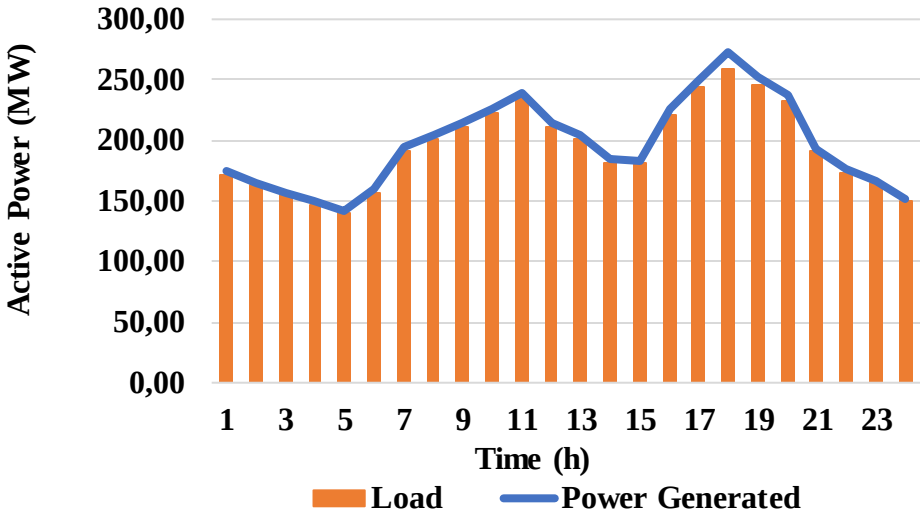

Figure 37 – Load curve for IEEE 14-bus test system.

Power flow simulations using the Newton method are performed for each case and to simulate uncertainties in the measurement chain, as before, an error of $\pm 1\%$ is considered for the voltage magnitude values.

4.3 Matpower Functios Used

Table 5 presents the Matpower functions used in the algorithm developed to perform the power flow studies, simulate PMU measurements and apply the methodologies tested in this work.

Table 5 – Matpower functions used and their descriptions.

Function	Description
loadcase()	Loads data from a Matpower case file or struct into data matrices or a case struct.
mpc.branch()	Used to access branch data of the loaded case.
mpc.bus()	Used to access and modify bus data, like loads associated with each bus, of the loaded case.
mpc.gen()	Used to access and modify generator data, like the power generation limits of each generator, of the loaded case.
runpf()	Runs the power flow algorithm for the loaded case. The results of power flow were stored in the struct “results”. The power flow method used was the Newton method.
results.bus()	Used to access and verify bus data used in power flow solution.

results.gen()	Used to access the calculated power produced by each generator by the power flow algorithm.
results.branch()	Used to retrieve information about the sending and receiving buses connected to each branch.

5. Results

In this section, the results for both case studies are presented and discussed.

5.1 Results For 5 Buses Radial Network Using The Nominal π Model Of A Transmission Line

The voltage and current magnitudes and phase angle calculated in the power flow solution and used to estimate the line parameters are presented in Table 6 and Table 7.

Table 6- Voltage magnitudes and phase angles of each bus obtained by power flow study.

Case	Bus 1		Bus 2		Bus 3		Bus 4		Bus 5	
	V (pu)	θ (degrees)	V (pu)	θ (degrees)	V (pu)	θ (degrees)	V (pu)	θ (degrees)	V (pu)	θ (degrees)
1	1	0	0,91	-10,45	0,89	-12,71	0,95	-5,21	1,01	1,83
2	1	0	0,89	-11,71	0,88	-14,29	0,95	-5,21	1,01	1,83
3	1	0	0,88	-13,04	0,86	-15,97	0,95	-5,21	1,01	1,83
4	1	0	0,90	-11,06	0,89	-13,36	0,94	-6,13	1,01	1,67
5	1	0	0,89	-11,69	0,88	-14,03	0,93	-7,07	1,01	1,52
6	1	0	0,90	-11,08	0,88	-13,62	0,94	-6,13	1,01	1,67
7	1	0	0,89	-11,72	0,87	-14,55	0,93	-7,07	1,01	1,52
8	1	0	0,91	-9,25	0,90	-11,22	0,94	-5,21	1,00	1,83
9	1	0	0,92	-8,11	0,90	-9,81	0,93	5,28	0,99	1,75
10	1	0	0,90	-9,85	0,88	-12,08	0,94	-4,30	0,99	1,98
11	1	0	0,90	-9,26	0,89	-11,46	0,94	-3,55	0,99	1,98
12	1	0	0,90	-9,84	0,88	-11,84	0,94	-4,19	0,99	2,09
13	1	0	0,91	-9,25	0,89	-10,99	0,94	-3,55	0,99	1,98
14	1	0	0,88	-11,71	0,86	-14,29	0,92	-6,13	0,99	1,67
15	1	0	0,86	-13,04	0,84	-15,97	0,91	-7,07	0,99	1,52
16	1	0	0,90	-9,25	0,89	-11,22	0,94	-4,30	0,99	1,98

17	1	0	0,92	-8,11	0,90	-9,81	0,94	-3,78	0,99	1,76
18	1	0	0,92	-7,55	0,91	-9,12	0,95	-3,52	0,99	1,65
19	1	0	0,91	-8,67	0,90	-10,51	0,94	-4,04	0,99	1,87
20	1	0	0,91	-8,96	0,89	-10,86	0,94	-4,17	0,99	1,93
21	1	0	0,91	-8,39	0,90	-10,15	0,94	-3,91	0,99	1,82
22	1	0	0,94	-7,94	0,92	-9,60	0,96	-3,70	1,01	1,73
23	1	0	0,94	-7,83	0,93	-9,46	0,96	-3,65	1,01	1,71
24	1	0	0,94	-7,71	0,93	-9,32	0,97	-3,60	1,01	1,69

Table 7- Sending and receiving end currents magnitude and phase angle obtained by power flow study for each branch.

Case	**Branch 1-2**				**Branch 1-5**			
	I1 (pu)	**ϕ1 (º)**	**I2 (pu)**	**ϕ2 (º)**	**I1 (pu)**	**ϕ1 (º)**	**I2 (pu)**	**ϕ2 (º)**
1	7,08	-29,61	7,08	150,34	4,96	6,80	4,96	-173,56
2	7,93	-31,05	7,93	148,91	4,96	6,80	4,96	-173,56
3	8,83	-32,58	8,83	147,38	4,96	6,80	4,96	-173,56
4	7,49	-30,20	7,49	149,76	4,54	6,74	4,54	-173,65
5	7,91	-30,80	7,91	149,15	4,13	6,69	4,12	-173,74
6	7,51	-30,45	7,51	149,50	4,54	6,74	4,54	-173,65
7	7,96	-31,33	7,96	148,63	4,13	6,69	4,12	-173,74
8	6,27	-28,24	6,27	151,70	4,96	6,80	4,96	-173,56
9	5,49	-26,92	5,49	153,01	4,76	6,77	4,76	-173,60
10	6,68	-29,04	6,68	150,91	5,37	6,87	5,37	-173,47
11	6,29	-28,49	6,29	151,46	5,38	6,87	5,38	-173,46
12	6,66	-28,80	6,66	151,15	5,67	6,91	5,67	-173,40
13	6,25	-28,02	6,25	151,92	5,38	6,87	5,38	-173,46
14	7,93	-31,05	7,93	148,91	4,54	6,74	4,54	-173,65
15	8,83	-32,58	8,83	147,38	4,13	6,69	4,12	-173,74
16	6,27	-28,24	6,27	151,70	5,37	6,87	5,37	-173,47
17	5,49	-26,93	5,49	153,01	4,78	6,78	4,78	-173,59
18	5,11	-26,28	5,11	153,65	4,49	6,74	4,48	-173,66
19	5,87	-27,58	5,88	152,36	5,08	6,83	5,07	-173,53
20	6,07	-27,91	6,07	152,03	5,22	6,84	5,22	-173,50
21	5,68	-27,25	5,68	152,69	4,93	6,80	4,96	-173,56
22	5,37	-26,73	5,38	153,20	4,69	6,77	4,69	-173,61
23	5,30	-26,61	5,30	153,33	4,63	6,76	4,63	-173,63
24	5,22	-26,48	5,22	153,46	4,57	6,75	4,57	-173,64

Case	Branch 2-3				Branch 4-5			
	I1 (pu)	ϕ1 (º)	I2 (pu)	ϕ2 (º)	I1 (pu)	ϕ1 (º)	I2 (pu)	ϕ2 (º)
1	3,57	-30,66	3,58	149,09	4,49	-23,32	4,49	156,60
2	4,01	-32,26	4,01	147,52	4,49	-23,32	4,49	156,60
3	4,47	-33,97	4,47	145,84	4,49	-23,32	4,49	156,60
4	3,60	-31,31	3,60	148,44	4,97	-24,26	4,98	155,67
5	3,63	-31,98	3,63	147,78	5,47	-25,21	5,48	154,73
6	3,97	-31,59	3,98	148,19	4,97	-24,26	4,98	155,67
7	4,39	-32,55	4,39	147,25	5,47	-25,21	5,48	154,73
8	3,16	-29,13	3,16	150,58	4,49	-23,32	4,49	156,60
9	2,76	-27,67	2,77	152,00	4,49	-23,40	4,49	156,52
10	3,54	-30,02	3,55	149,72	4,00	-22,41	4,01	157,51
11	3,52	-29,40	3,52	150,34	3,53	-21,65	3,54	158,25
12	3,18	-29,75	3,19	149,97	4,00	-22,30	4,01	157,62
13	2,80	-28,86	2,80	150,81	3,53	-21,65	3,54	158,25
14	4,01	-32,26	4,01	147,52	4,97	-24,26	4,98	155,67
15	4,47	-33,97	4,47	145,84	5,47	-25,21	5,48	154,73
16	3,16	-29,13	3,16	150,58	4,00	-22,41	4,01	157,51
17	2,76	-27,67	2,77	152,00	3,53	-21,87	3,54	158,03
18	2,57	-26,95	2,57	152,68	3,30	-21,61	3,30	158,29
19	2,96	-28,39	2,96	151,30	3,77	-22,14	3,77	157,77
20	3,06	-28,76	3,06	150,94	3,89	-22,27	3,89	157,64
21	2,86	-28,03	2,86	151,65	3,65	-22,00	3,65	157,90
22	2,70	-27,45	2,71	152,21	3,46	-21,79	3,47	158,11
23	2,66	-27,31	2,67	152,34	3,42	-21,74	3,42	158,16
24	2,63	-27,17	2,63	152,48	3,37	-21,68	3,37	158,21

Before presenting the line parameters estimated using the nominal π model methodology explained earlier, load and power diagrams, tangent of phi of all loads and power loss throughout the twenty-four simulated scenarios are shown.

Figure 38 shows the active load diagram by each load through the cases simulated.

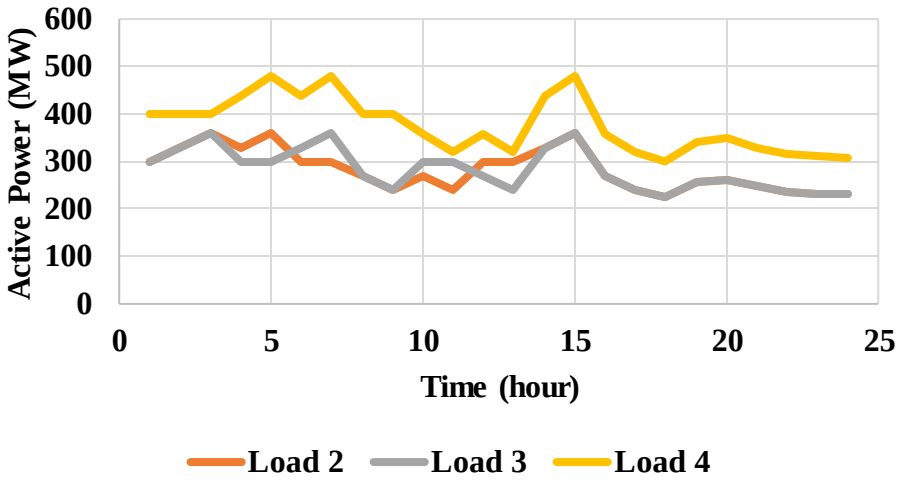

Figure 38- Active load diagram.

As Figure 38 shows, the active loads of the system were modified during the simulations to simulate the behavior of a real power system.

Figure 39 shows the reactive load diagram by each load through the cases simulated. The reactive loads were also modified during the simulations to simulate the behavior of a real power system.

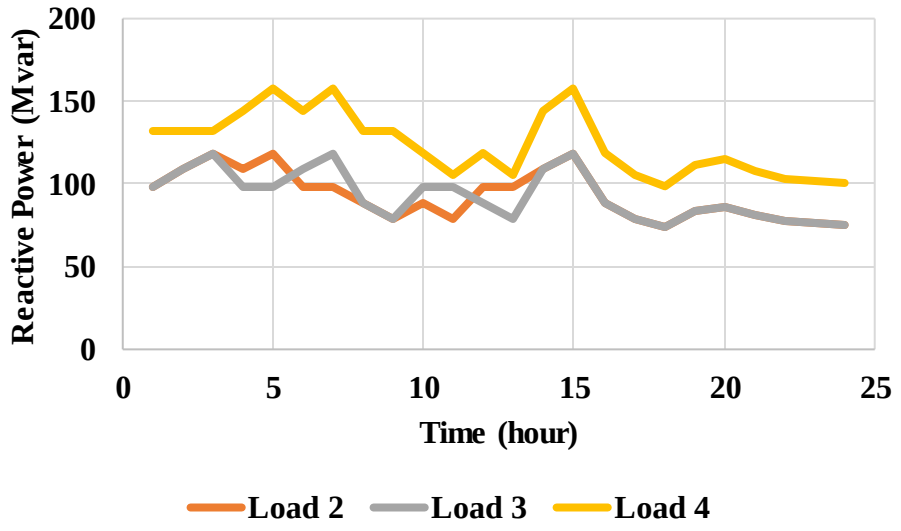

Figure 39- Reactive load diagram.

Annex B shows the variation of the tangent of phi of loads 2, 3 and 4 through time. Their tangent of phi was 0,33 all the time as loads were dimensioned to have a good power factor, something of importance in a real power system as impacts on its efficiency.

Power diagrams of the generators are shown in Figure 40 and Figure 41.

Figure 40 shows the diagram of active power generated by each generator throughout the scenarios simulated. Generator 1, located at the slack bus, acts as a complement to generator 5 in all scenarios.

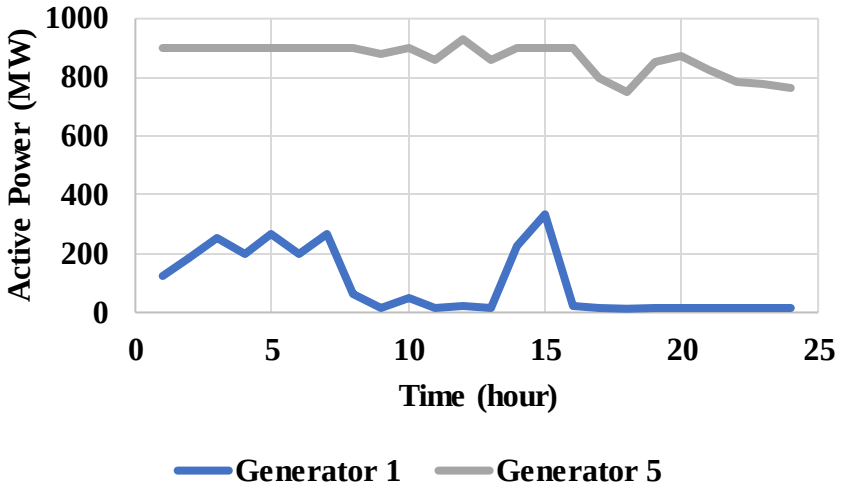

Figure 40- Active power generation diagram.

Figure 41 presents the reactive power generation diagram. Generator 1 supplies most of the reactive power required by the system and generator 5 complements it. None of the generators absorbs reactive power from the system.

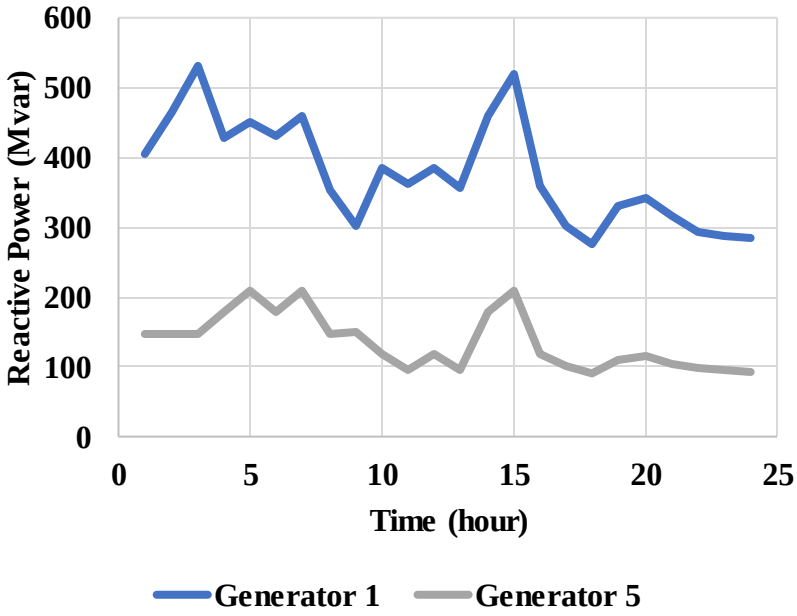

Figure 41- Reactive power generation diagram.

Typical power loss in transmission lines is around 2% to 4% of the generated

power. As Figure 42 shows, the total active power loss in the system varied between 1,6% and 2,7% of the generated power. In most of the cases it was superior to 2%.

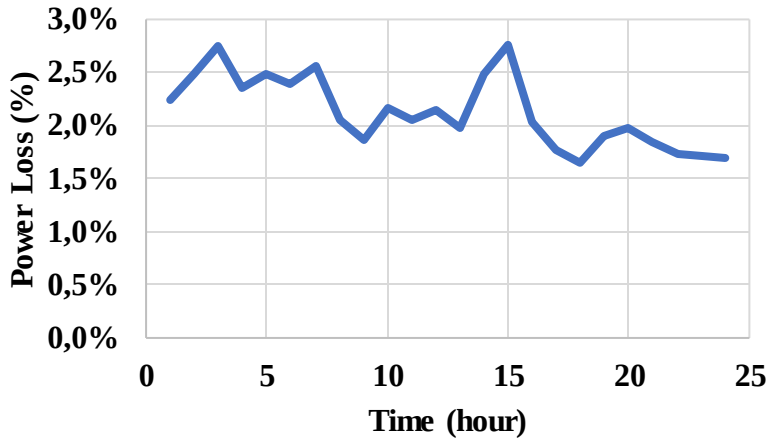

Figure 42- Active power loss.

A comparison between total reactive power generated and consumed is also made in Figure 43 and the difference between the two is shown in Figure 44.

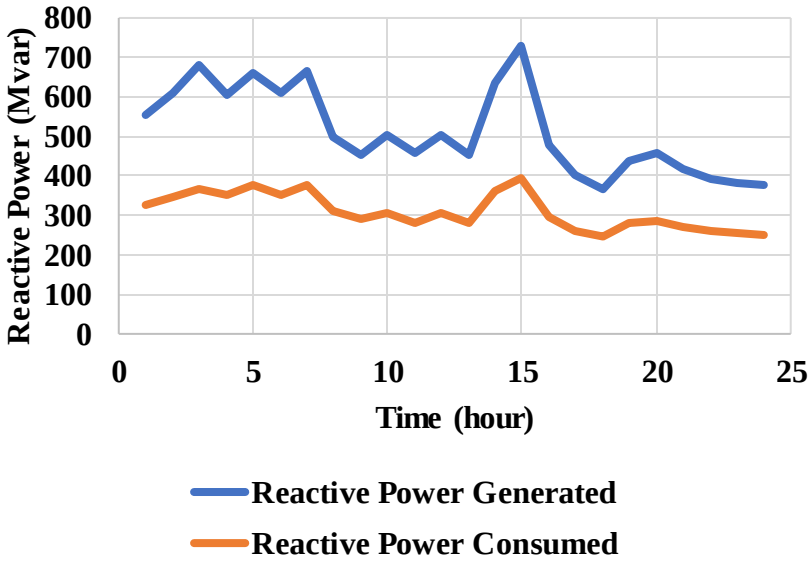

Figure 43- Total reactive power generated vs total reactive power consumed.

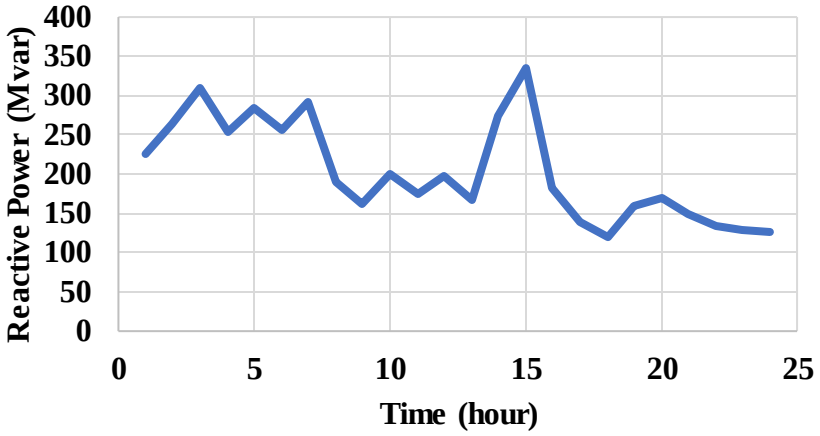

Figure 44- Reactive power difference.

Now, the results from the using the nominal π model are presented. Estimated line parameters are compared to the nominal values and discussed.

Table 8 compares the estimated line resistance to the nominal value.

Table 8- Lumped series resistances of the lines.

Line	*R* nominal (pu)	*R* estimated (mean value) (pu)	Relative error	Standard Deviation
1-2	0,00281	0,00304	8,21%	$1{,}3\ x\ 10^{-3}$
1-5	0,00064	0,00191	197,85%	$7{,}7\ x\ 10^{-4}$
2-3	0,00108	0,00108	0,13%	$1\ x\ 10^{-5}$
4-5	0,00297	0,00297	0,13%	$2{,}9\ x\ 10^{-5}$

As Table 8 shows, not all values of resistance calculated were calculated with good precision as the series resistance of line 1-5 had a remarkably high relative error to the original resistance. The introduced errors in voltage values had a particular high impact on this line parameters identification.

The relative errors for lines 1-2 and 1-5 were the highest and to see the change in value over time there are Figure 45 and Figure 46.

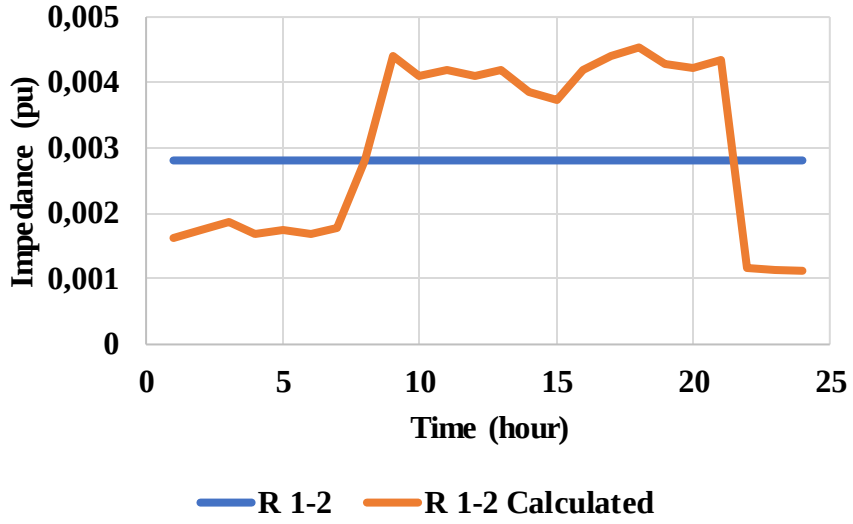

Figure 45 – Line 1-2 series resistance over time.

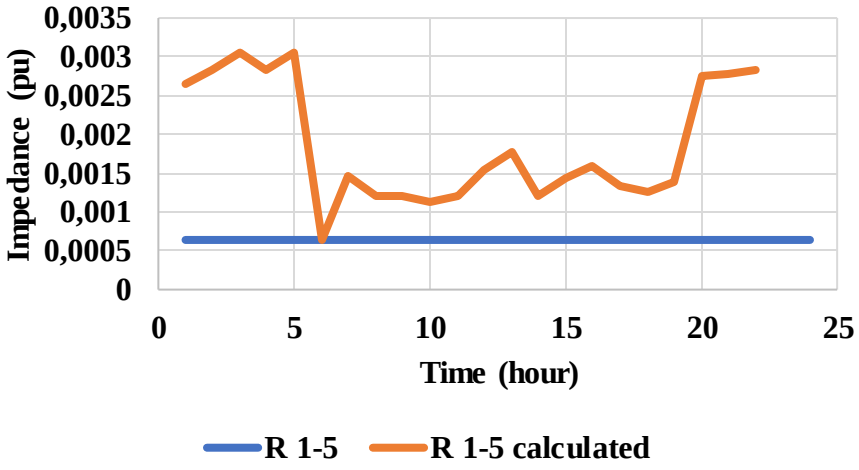

Figure 46 - Line 1-5 series resistance over time.

Table 9 shows that the series reactances estimated had low relative error compared to the nominal value and low standard deviation. Even with errors introduced, a precise estimation of the reactances was possible.

Table 9 – Lumped series reactances of the lines.

Line	X nominal (pu)	X estimated (mean value) (pu)	Relative error	Standard Deviation
1-2	0,0281	0,0282	0,28%	$4{,}5\ x\ 10^{-4}$
1-5	0,0064	0,0064	0,22%	$1{,}7\ x\ 10^{-4}$
2-3	0,0108	0,0108	0,12%	$1{,}1\ x\ 10^{-4}$

4-5	0,0297	0,0297	0,12%	$2{,}9\ x\ 10^{-4}$

The same applies to the results shown in Table 10. The shunt susceptance of the lines could be estimated with low relative errors and low standard deviations compared to the nominal values.

Table 10 – Lumped shunt susceptance of the lines.

Line	**B nominal (pu)**	**B estimated (mean value) (pu)**	**Relative error**	**Standard Deviation**
1-2	0,00712	0,00712	0,06%	$3{,}3\ x\ 10^{-5}$
1-5	0,03126	0,03128	0,06%	$1{,}5\ x\ 10^{-4}$
2-3	0,01852	0,01855	0,13%	$1{,}8\ x\ 10^{-4}$
4-5	0,00674	0,00675	0,13%	$6{,}5\ x\ 10^{-5}$

In general, as expected, resistance had a higher variation then the other line parameters, especially for lines 1-2 and 1-5, where the generators were connected. Line 1-5 had the highest variation from the original value. However, considering series reactance and shunt susceptance, the estimations were done with good precision regardless of the errors introduced.

Regarding conductance, it was considered null when running power flows, but calculating the parameters a small value was found for each branch in each scenario.

Table 11 presents the average conductance calculated for each line.

Table 11- Lumped shunt conductance for each line.

Line	**G estimated (mean value) (pu)**
1-2	$2{,}9\ x\ 10^{-6}$
1-5	$2{,}3\ x\ 10^{-6}$
2-3	$2{,}25\ x\ 10^{-15}$
4-5	$1{,}25\ x\ 10^{-16}$

As Table 11 shows, the conductance values found are so small that they can be omitted when modeling the system, as it usually occurs.

5.2 Results For IEEE 14-Bus Test System

The voltage and current magnitudes and phase angles calculated in the power flow solution and used to estimate the line parameters are presented in Table 12, Table 13 and Table 14.

Table 12- Voltage magnitudes and phase angles of each bus obtained by power flow study of the 14 bus IEEE network.

Case	Bus 1		Bus 2		Bus 3		Bus 4		Bus 5	
	V (pu)	θ (degrees)	V (pu)	θ (degrees)	V (pu)	θ (degrees)	V (pu)	θ (degrees)	V (pu)	θ (degrees)
1	1,05	0	1,03	-0,33	1,00	-2,26	1,00	-3,25	1,01	-2,79
2	1,05	0	1,03	-0,12	1,00	-1,78	1,00	-2,87	1,01	-2,46
3	1,07	0	1,06	0,08	1,02	-1,32	1,02	-2,52	1,03	-2,16
4	1,07	0	1,06	0,26	1,02	-0,89	1,03	-2,18	1,03	-1,87
5	1,07	0	1,06	0,44	1,02	-0,49	1,03	-1,86	1,03	-1,59
6	1,07	0	1,06	0,03	1,02	-1,43	1,02	-2,60	1,03	-2,23
7	1,07	0	1,06	-0,79	1,02	-3,33	1,02	-4,08	1,03	-3,51
8	1,07	0	1,06	-1,03	1,02	-3,86	1,02	-4,50	1,03	-3,87
9	1,06	0	1,05	-1,27	1,01	-4,43	1,01	-4,94	1,02	-4,25
10	1,05	0	1,03	-1,56	1,00	-5,09	1,00	-5,46	1,00	-4,69
11	1,05	0	1,03	-1,85	1,00	-5,76	0,99	-5,98	1,00	-5,14
12	1,05	0	1,03	-1,29	1,00	-4,46	1,00	-4,96	1,01	-4,27
13	1,05	0	1,03	-1,03	1,00	-3,86	1,00	-4,50	1,01	-3,87
14	1,07	0	1,06	-0,57	1,02	-2,82	1,02	-3,68	1,03	-3,16
15	1,05	0	1,03	-0,55	1,00	-2,76	1,00	-3,64	1,01	-3,13
16	1,05	0	1,03	-1,53	1,00	-5,03	1,00	-5,41	1,00	-4,65
17	1,05	0	1,03	-1,83	1,00	-6,32	0,99	-6,42	1,00	-5,52
18	1,05	0	1,03	-5,00	1,00	-12,81	1,00	-10,24	1,01	-8,73
19	1,05	0	1,03	-2,16	1,00	-6,46	0,99	-6,53	1,00	-5,62
20	1,05	0	1,03	-1,81	1,00	-5,66	0,99	-5,90	1,00	-5,08
21	1,05	0	1,03	-0,78	1,00	-3,30	1,00	-4,06	1,01	-3,49
22	1,07	0	1,06	-0,36	1,02	-2,33	1,02	-3,30	1,03	-2,83
23	1,07	0	1,06	-0,16	1,02	-1,87	1,02	-2,94	1,03	-2,52
24	1,07	0	1,06	0,21	1,02	-1,02	1,03	-2,28	1,03	-1,95

Table 13- Current injections magnitudes and phase angles of each bus obtained by power flow study of the 14 bus IEEE network

Case	Bus 1		Bus 2		Bus 3		Bus 4		Bus 5	
	I (pu)	ϕ (degrees)	I (pu)	ϕ (degrees)	I (pu)	ϕ (degrees)	I (pu)	ϕ (degrees)	I (pu)	ϕ (degrees)
1	0,50	-33,07	0,63	0,74	0,24	118,41	0,34	154,96	0,05	155,47
2	0,44	-41,10	0,64	2,53	0,24	110,72	0,32	155,33	0,05	155,78
3	0,40	-50,55	0,64	4,14	0,25	103,57	0,30	155,69	0,05	156,09
4	0,38	-61,17	0,65	5,60	0,25	97,12	0,29	156,02	0,05	156,37
5	0,36	-72,30	0,66	6,91	0,26	91,45	0,27	156,34	0,04	156,65
6	0,41	-48,09	0,64	3,76	0,25	105,27	0,31	155,60	0,05	156,01
7	0,65	-20,79	0,61	-3,57	0,26	134,57	0,38	154,13	0,06	154,76
8	0,73	-16,65	0,61	-5,90	0,28	141,61	0,39	154,13	0,06	154,41
9	0,82	-13,23	0,60	-8,47	0,30	148,05	0,42	153,27	0,07	154,04
10	0,93	-10,15	0,60	-14,91	0,33	154,31	0,44	152,75	0,07	153,61
11	1,04	-7,74	0,59	-14,91	0,36	159,47	0,46	152,24	0,07	153,18
12	0,82	-13,08	0,60	-8,60	0,30	148,34	0,42	153,25	0,07	154,02
13	0,73	-16,66	0,61	-5,89	0,30	141,59	0,39	153,25	0,06	154,41
14	0,57	-25,85	0,63	-1,45	0,25	127,14	0,36	154,52	0,06	155,42
15	0,57	-21,04	0,62	-1,24	0,25	126,34	0,36	154,57	0,06	155,13
16	0,92	-10,41	0,60	-11,31	0,32	153,78	0,44	152,80	0,07	153,65
17	1,14	-6,09	0,59	-17,82	0,39	163,07	0,46	151,79	0,08	152,82
18	2,20	3,53	0,40	-69,22	0,94	173,36	0,48	174,42	0,08	159,38
19	1,16	-5,74	0,59	-18,55	0,40	163,86	0,49	151,69	0,08	152,73
20	1,02	-8,06	0,59	-14,42	0,35	158,78	0,46	152,31	0,07	153,24
21	0,64	-21,04	0,61	-3,44	0,26	134,17	0,37	154,15	0,06	154,78
22	0,51	-31,99	0,63	0,46	0,24	119,58	0,34	154,90	0,05	155,42
23	0,45	-39,39	0,63	2,19	0,24	112,21	0,32	155,26	0,05	155,72
24	0,38	-57,94	0,65	5,18	0,25	98,95	0,29	155,93	0,05	156,29

Table 14- Sending and receiving end currents magnitude and phase angle obtained by power flow study for each branch of the 14 bus IEEE network.

Case	Branch 1-2				Branch 1-5				Branch 2-3	
	I1 (pu)	ϕ1 (º)	I2 (pu)	ϕ2 (º)	I1 (pu)	ϕ1 (º)	I2 (pu)	ϕ2 (º)	I1 (pu)	ϕ1 (º)
1	0,24	-45,91	0,28	126,17	0,27	-21,81	0,29	149,76	0,23	-29,21

2	0,22	-60,39	0,27	113,73	0,25	-24,20	0,27	146,86	0,21	-33,07
3	0,21	-75,66	0,27	101,42	0,23	-26,95	0,25	143,64	0,20	-37,39
4	0,23	-89,66	0,28	90,30	0,21	-30,11	0,23	140,09	0,19	-42,14
5	0,25	-101,18	0,30	80,91	0,19	-33,72	0,22	136,21	0,18	-47,31
6	0,21	-71,93	0,27	104,38	0,23	-26,24	0,26	144,47	0,20	-36,28
7	0,32	-23,77	0,35	147,83	0,32	-17,83	0,34	154,78	0,27	-22,62
8	0,38	-16,93	0,40	155,36	0,35	-16,34	0,37	156,74	0,30	-20,12
9	0,44	-11,66	0,45	161,43	0,38	-15,05	0,39	158,48	0,32	-17,93
10	0,52	-7,21	0,52	166,75	0,41	-13,82	0,43	160,17	0,35	-15,85
11	0,59	-3,91	0,60	170,78	0,45	-12,82	0,46	161,59	0,38	-14,15
12	0,44	-11,44	0,46	161,69	0,38	-14,99	0,39	158,56	0,32	-17,83
13	0,38	-16,95	0,40	155,34	0,35	-16,35	0,37	156,73	0,30	-20,13
14	0,28	-32,65	0,31	138,67	0,30	-19,53	0,32	152,60	0,25	-25,46
15	0,27	-33,72	0,31	137,61	0,30	-19,72	0,31	152,35	0,25	-25,78
16	0,51	-7,56	0,52	166,32	0,38	-13,93	0,42	158,48	0,35	-16,03
17	0,66	-1,76	0,67	173,45	0,48	-12,12	0,49	162,61	0,41	-12,96
18	1,50	7,44	1,49	-174,67	0,71	-4,69	0,71	171,67	0,71	-8,00
19	0,68	-1,30	0,68	174,02	0,48	-11,97	0,49	162,84	0,41	-12,70
20	0,58	-4,34	0,59	170,25	0,44	-12,96	0,45	161,40	0,38	-14,38
21	0,32	-24,20	0,35	147,37	0,32	-17,92	0,34	154,67	0,27	-22,76
22	0,24	-43,92	0,28	127,96	0,28	-21,48	0,29	147,46	0,23	-28,67
23	0,22	-57,39	0,27	116,22	0,25	-23,70	0,27	147,46	0,20	-32,27
24	0,22	-85,75	0,28	93,42	0,21	-29,13	0,24	141,18	0,19	-40,69

Case	**Branch 2-3**		**Branch 2-4**				**Branch 2-5**			
	I2 (pu)	**ϕ2 (º)**	**I1 (pu)**	**ϕ1 (º)**	**I2 (pu)**	**ϕ2 (º)**	**I1 (pu)**	**ϕ1 (º)**	**I2 (pu)**	**ϕ2 (º)**
1	0,25	143,05	0,33	-10,81	0,34	160,68	0,27	-9,35	0,28	163,56
2	0,24	139,04	0,31	-10,92	0,32	160,14	0,26	-9,23	0,27	163,37
3	0,22	134,73	0,29	-11,08	0,31	159,54	0,25	-9,14	0,26	163,14
4	0,21	130,16	0,28	-11,29	0,29	158,87	0,24	-9,08	0,25	162,86
5	0,21	125,40	0,26	-11,55	0,28	158,14	0,23	-9,06	0,24	162,54
6	0,23	135,82	0,30	-11,23	0,31	159,69	0,25	-9,15	0,26	163,20
7	0,29	150,25	0,36	-10,73	0,37	161,58	0,30	-9,73	0,31	163,80
8	0,31	153,11	0,38	-10,77	0,39	161,91	0,32	-9,96	0,32	163,85
9	0,33	155,67	0,40	-10,85	0,41	162,17	0,33	-10,23	0,34	163,84
10	0,36	158,17	0,43	-11,00	0,43	162,40	0,35	-10,58	0,35	163,78
11	0,39	160,27	0,45	-11,19	0,46	162,54	0,36	-10,95	0,37	163,67
12	0,33	155,79	0,40	-10,86	0,41	162,18	0,33	-10,25	0,34	163,84
13	0,31	155,79	0,38	-10,77	0,39	161,91	0,32	-9,96	0,32	163,85

14	0,27	147,09	0,35	-10,74	0,36	161,20	0,29	-9,53	0,30	163,72
15	0,27	146,74	0,34	-10,75	0,35	161,15	0,29	-9,52	0,29	163,71
16	0,36	157,96	0,42	-10,98	0,43	162,38	0,35	-10,54	0,35	163,79
17	0,41	161,77	0,47	-11,38	0,48	162,61	0,38	-11,29	0,38	163,69
18	0,71	168,89	0,54	-7,36	0,54	167,29	0,40	-10,19	0,40	164,82
19	0,42	162,10	0,47	-11,43	0,48	162,62	0,38	-11,37	0,39	163,50
20	0,38	159,99	0,44	-11,16	0,45	162,53	0,36	-10,54	0,37	163,69
21	0,29	150,09	0,36	-10,73	0,37	161,56	0,30	-9,72	0,31	163,80
22	0,25	143,63	0,33	-10,80	0,34	160,75	0,28	-9,37	0,28	163,59
23	0,24	139,86	0,31	-10,89	0,32	160,25	0,27	-9,25	0,27	163,41
24	0,22	131,54	0,28	-11,23	0,30	159,07	0,24	-9,09	0,25	162,94

After presenting load and power diagrams, tangent of phi of all loads and power loss throughout the twenty-four simulated scenarios are shown, the line parameters estimated using the nominal π model and the admittance matrix identification methodologies are presented.

Active and reactive load diagrams representing load changes through time are shown in Figure 47 and Figure 48.

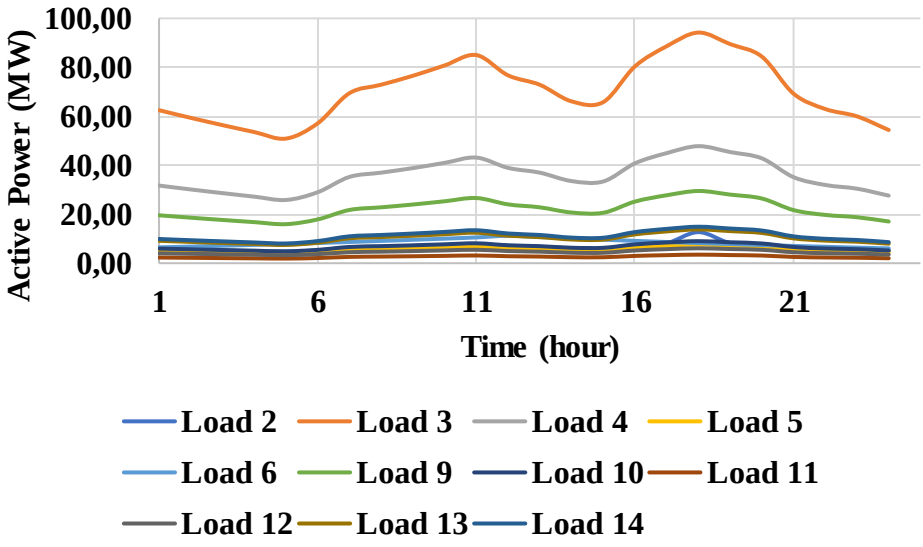

Figure 47 – Active load diagram.

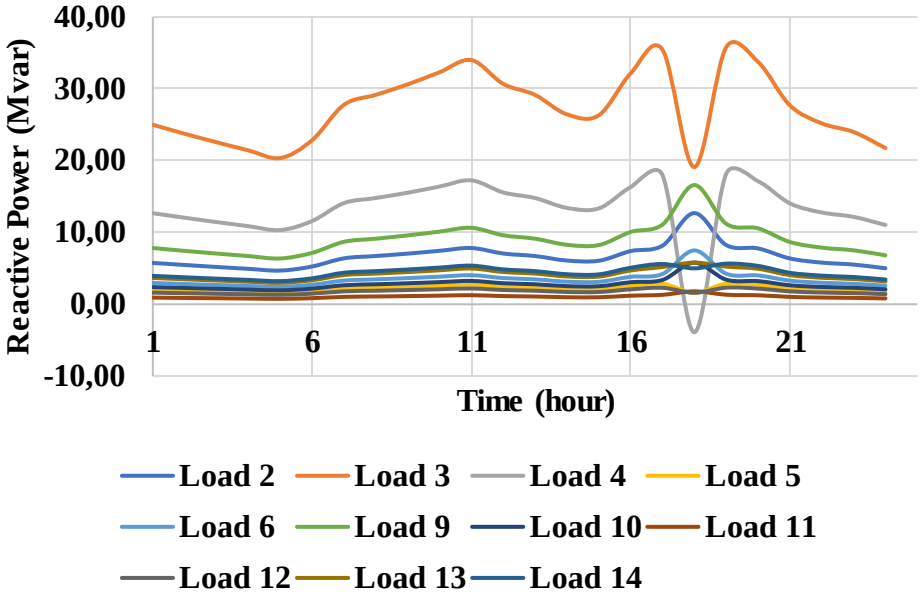

Figure 48- Reactive load diagram.

The tangent phi of the loads through time were monitored and are shown in Annex C. The original system data has loads of varied tangent phi values that sometimes represented bad power factors, which is not desirable. Thus, in the other cases constructed the power of the loads were altered to achieve a good power factor.

Active and reactive power generation of the generators and synchronous compensators are presented hourly in Figure 49 and Figure 50.

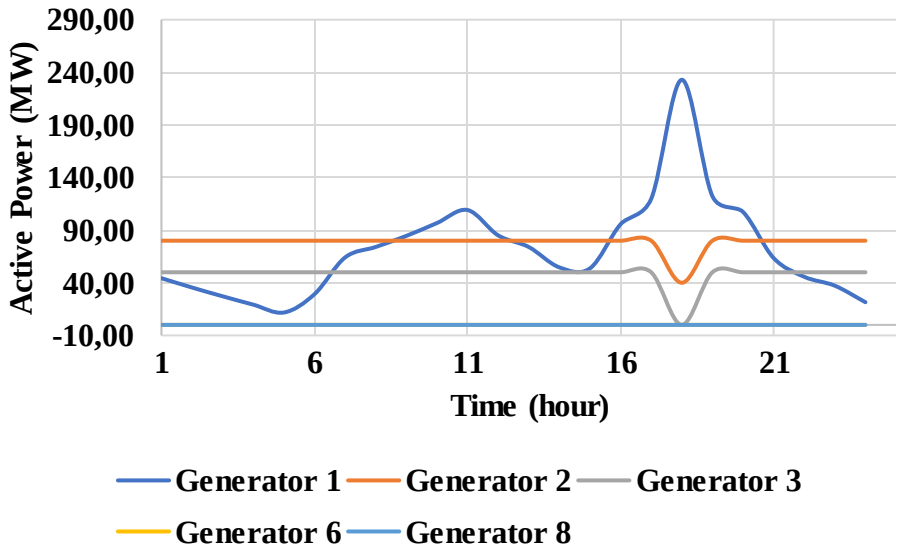

Figure 49 – Active power generated.

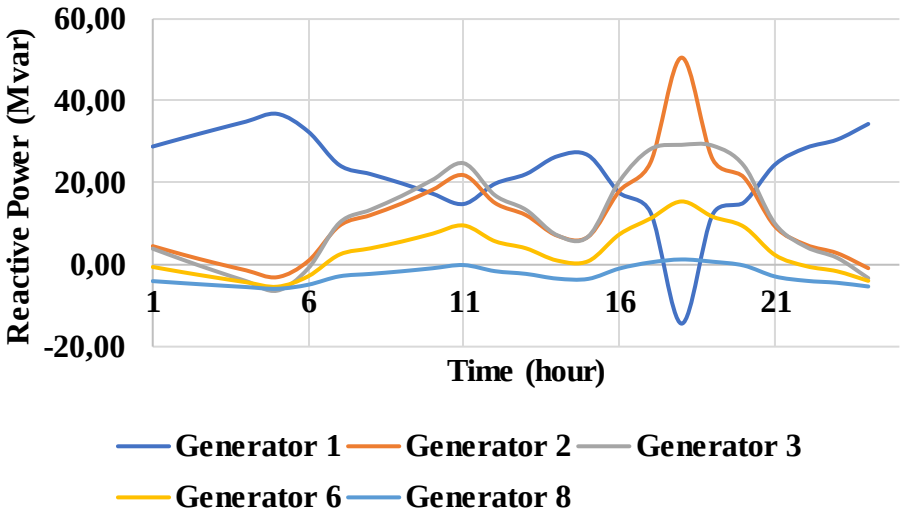

Figure 50 – Reactive power generated.

The total active power loss in the network was tracked and is shown in Figure 51.

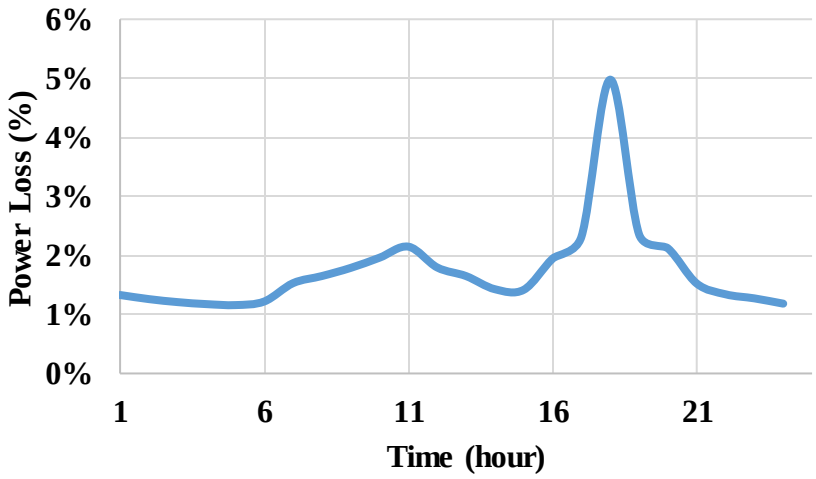

Figure 51- Total active power loss.

The active power loss varied from close to 1% to 5% of the active power generated and the average power loss was of 2%. The highest power loss occurred when the true load characteristics of the system were used. When modifying the loads to have a good tangent of phi, the efficiency of the system improved and most of the losses were lower than of real power systems.

The results for the line parameters estimation methodologies are divided into the next two sections for better understanding.

5.2.1 Results For IEEE 14-Bus Test System Using The Nominal π Model Of A Transmission Line

The lumped parameters for selected lines are obtained for the 24-hour time series, and their mean value, relative error and standard deviation are presented in Table 15, Table 16 and Table 17 for the series resistance, series reactance and shunt susceptance, respectively.

Results for series resistance shown in Table 15 are much better than the ones obtained for the radial power system as the relative errors to nominal values are low in all cases. Line 2-4 presented the highest relative error and standard deviation, but it still was low.

Table 15- Lumped series resistances of selected lines.

Line	***R* nominal (pu)**	***R* estimated (mean value) (pu)**	**Relative error**	**Standard Deviation**
1-2	0,01938	0,01936	0,13%	$1{,}9\ x\ 10^{-4}$
1-5	0,05403	0,05396	0,12%	$5{,}2\ x\ 10^{-4}$
2-3	0,04699	0,04693	0,13%	$4{,}6\ x\ 10^{-4}$
2-4	0,05869	0,05804	1,11%	$5{,}6\ x\ 10^{-4}$
2-5	0,05695	0,05688	0,13%	$5{,}5\ x\ 10^{-4}$

Table 16, as Table 9, shows the good precision for series reactance calculation, but in this test one of the lines series reactance could be calculated with almost no error.

Table 16 – Lumped series reactances of selected lines.

Line	**X nominal (pu)**	**X estimated (mean value) (pu)**	**Relative error**	**Standard Deviation**
1-2	0,05917	0,05910	0,13%	$5{,}7\ x\ 10^{-4}$
1-5	0,22304	0,22276	0,12%	$2{,}2\ x\ 10^{-3}$
2-3	0,19797	0,19797	0,00%	$5{,}5\ x\ 10^{-17}$
2-4	0,17632	0,17610	0,13%	$1{,}7\ x\ 10^{-3}$
2-5	0,17388	0,17366	0,13%	$1{,}7\ x\ 10^{-3}$

Table 17, as Table 10, also shows a good result for line shunt susceptances. The relative errors and standard deviations are very low.

Table 17 – Lumped series susceptances of selected lines.

Line	*B* nominal (pu)	*B* estimated (mean value) (pu)	Relative error	Standard Deviation
1-2	0,0528	0,0529	0,13%	$5{,}1\ x\ 10^{-4}$
1-5	0,0438	0,0439	0,13%	$4{,}3\ x\ 10^{-4}$
2-3	0,0374	0,0375	0,13%	$3{,}6\ x\ 10^{-4}$
2-4	0,0492	0,0493	0,13%	$4{,}8\ x\ 10^{-4}$
2-5	0,0340	0,0341	0,13%	$3{,}3\ x\ 10^{-4}$

The results from Table 15, Table 16 and Table 17 shows that even with the insertion of measurement errors the methodology based on the nominal π model of a transmission line proved useful for estimating line parameters with good precision.

As said earlier, shunt conductance is usually neglected when modeling a transmission line by the nominal π model. This is attested by Table 18, as Table 11 also does.

Table 18 – Lumped shunt conductance for selected lines.

Line	G estimated (mean value) (pu)
1-2	$2{,}38\ x\ 10^{-16}$
1-5	$1{,}49\ x\ 10^{-17}$
2-3	$9{,}93\ x\ 10^{-17}$
2-4	$1{,}05\ x\ 10^{-16}$
2-5	$7{,}95\ x\ 10^{-17}$

5.2.2 Results For IEEE 14-Bus Test System Line Parameters Estimation By Admittance Matrix Identification

Regarding the methodology that infers the nodal admittance matrix based on a set of phasor measurements, it was possible to estimate the values of the series resistance and series reactance of the branches.

Table 19 and Table 20 present the estimated series resistances and reactances of some of the lines of the network, respectively.

Table 19- Estimated series resistances.

Line	Nominal *R* (pu)	Estimated *R* (pu)	Relative error
1-2	0,01938	0,01920	1%
1-5	0,05403	0,04816	11%
2-3	0,04699	0,04309	8%
2-4	0,05869	0,06188	5%
2-5	0,05695	0,05566	2%

Table 20 – Estimated series reactances.

Line	Nominal *X* (pu)	Estimated *X* (pu)	Relative error
1-2	0,05917	0,05835	1%
1-5	0,22304	0,22158	1%
2-3	0,19797	0,19669	1%
2-4	0,17632	0,16696	5%
2-5	0,17388	0,16391	6%

As Table 19 and Table 20 showed, it was possible to estimate the series parameters of the lines with a high accuracy of within 1% of the original value. However, in certain cases, the method's accuracy varied, with the most inaccurate data showing a relative error of 11% of the nominal value.

It is important to note that the shunt parameters estimated by this method do not align with the expected results. However, if the system lines are relatively short, only the series resistances and reactances of the lines are of importance.

To further evaluate this methodology, a sensibility analysis is discussed in the next subsection.

5.2.2.1 Sensibility Analysis

For a better understanding of how the quantity of available phasor measurements affect the results obtained by admittance matrix identification, the methodology was employed again for 12 and 240 set of measurements in the load curve of Figure 37.

Table 21 to Table 24 present the estimated series resistances and reactances estimated through each new set of measurements.

Table 21- Estimated series resistances with 12 measurements.

Line	Nominal *R* (pu)	Estimated *R* (pu)	Relative error
1-2	0,01938	0,01925	0,69%
1-5	0,05403	0,04736	12,35%
2-3	0,04699	0,04248	9,59%
2-4	0,05869	0,06194	5,54%
2-5	0,05695	0,05643	0,91%

Table 22- Estimated series reactances with 12 measurements.

Line	Nominal *X* (pu)	Estimated *X* (pu)	Relative error
1-2	0,05917	0,05837	1,35%
1-5	0,22304	0,22006	1,34%
2-3	0,19797	0,19674	0,62%
2-4	0,17632	0,16618	5,75%
2-5	0,17388	0,16214	6,75%

Table 23 – Estimated series resistances with 240 measurements.

Line	Nominal *R* (pu)	Estimated *R* (pu)	Relative error
1-2	0,01938	0,01897	2,10%
1-5	0,05403	0,04980	7,83%
2-3	0,04699	0,04258	9,37%
2-4	0,05869	0,05879	0,18%
2-5	0,05695	0,05743	0,86%

Table 24 – Estimated series reactances with 240 measurements.

Line	Nominal *X* (pu)	Estimated *X* (pu)	Relative error
1-2	0,05917	0,05839	1,35%
1-5	0,22304	0,22233	1,34%
2-3	0,19797	0,19599	0,62%
2-4	0,17632	0,16775	5,75%
2-5	0,17388	0,16580	6,75%

Table 21 to Table 24 show that the results get better with the greater number of measurements and that can be better seen on Table 25, which compares the average errors of estimated resistances and reactances obtained with each set of measurements studied.

Table 25- Comparison of average absolute errors between sets of measurements studied.

Number of measurements	Average absolute R estimated error	Average absolute X estimated error
12	5,8%	3,2%
24	5,5%	2,7%
240	4,1%	2,4%

Therefore, the number of available measurements may affect the final result of the method and is something that needs to be considered when applying it. The test done shows that the precision of the algorithm increases with the number of measurements available.

6. Conclusion

Accurate transmission line parameter values are crucial for maintaining the stability and security of the power grid. However, traditional methods that rely on theoretical formulas based on the physical attributes and material properties of the lines may not account for changes in these parameters over time due to factors like environmental conditions and aging components. These changes can impact the precision of real-time system operations and long-term applications. Therefore, it is vital to employ estimation techniques for transmission line parameters.

This study introduces two approaches for identifying the parameters of the equivalent π model of transmission lines. Results obtained using the methodologies presented showed a satisfactory level of accuracy for series resistance and reactance estimation. However, the results obtained by the methodology based solely on Kirchoff's law and the characteristic equations of the equivalent π model of the transmission line were far better than the methodology based on admittance matrix identification. Another difference between the two methodologies is that the first was capable of estimating shunt parameters with good precision while the second could not identify these parameters and

the sensitivity analysis done showed that precision of that method is tied to the quantity of phasor measurements available to every bus. Thus, further research is necessary to refine this aspect of the methodology.

Additionally, the first method approached can be used for online estimation of transmission line parameters but is restricted to lines where the buses at both ends of the line have phasor measurements available. Meanwhile, the second approach has the drawback of only being suitable for fully observable power systems. Moreover, it is important to acknowledge that not all buses in practical power systems have monitoring capabilities, and the installation of PMUs can be costly. Therefore, future research should concentrate on developing techniques for estimating line parameters in networks where phasor measurements are not available at every bus.

References

[1] B. Patel and P. Bera, "A New Transmission Line Parameter Estimation Technique and Its Impact on Fault Localization," *IEEE Trans. Instrum. Meas.*, vol. 72, pp. 1–8, 2023, doi: 10.1109/TIM.2023.3301889.

[2] Y. Wang, M. Xia, Q. Yang, Y. Song, Q. Chen, and Y. Chen, "Augmented State Estimation of Line Parameters in Active Power Distribution Systems With Phasor Measurement Units," *IEEE Trans. Power Deliv.*, vol. 37, no. 5, pp. 3835–3845, Oct. 2022, doi: 10.1109/TPWRD.2021.3138165.

[3] L. F. Costa, J. S. Giraldo, and C. A. Castro, "Identification and correction of transmission line parameter errors using SCADA and synchrophasor measurements," *Int. J. Electr. Power Energy Syst.*, vol. 135, p. 107509, Feb. 2022, doi: 10.1016/j.ijepes.2021.107509.

[4] J. Sun, M. Xia, and Q. Chen, "A Classification Identification Method Based on Phasor Measurement for Distribution Line Parameter Identification Under Insufficient Measurements Conditions," *IEEE Access*, vol. 7, pp. 158732–158743, 2019, doi: 10.1109/ACCESS.2019.2950461.

[5] A. Momen, Y. Chakhchoukh, and B. K. Johnson, "Series Compensated Line Parameters Estimation Using Synchrophasor Measurements," *IEEE Trans. Power Deliv.*, vol. 34, no. 6, pp. 2152–2162, Dec. 2019, doi: 10.1109/TPWRD.2019.2915992.

[6] S. S. Mousavi-Seyedi, F. Aminifar, and S. Afsharnia, "Parameter Estimation of Multiterminal Transmission Lines Using Joint PMU and SCADA Data," *IEEE Trans. Power Deliv.*, vol. 30, no. 3, pp. 1077–1085, Jun. 2015, doi: 10.1109/TPWRD.2014.2369500.

[7] A. Xue, F. Xu, K. E. Martin, J. Xu, H. You, and T. Bi, "Linear Approximations for the Influence of Phasor Angle Difference Errors on Line Parameter Calculation," *IEEE Trans. Power Syst.*, vol. 34, no. 5, pp. 3455–3464, Sep. 2019, doi: 10.1109/TPWRS.2019.2902885.

[8] J. Lin, J. Song, and C. Lu, "Synchrophasor Data Analytics: Transmission Line

Parameters Online Estimation for Energy Management," *IEEE Trans. Eng. Manag.*, vol. 69, no. 3, pp. 671–681, Jun. 2022, doi: 10.1109/TEM.2019.2939173.
[9] C. Laurano, P. A. Pegoraro, C. Sitzia, A. V. Solinas, S. Sulis, and S. Toscani, "Refined Modeling and Compensation of Current Transformers Behavior for Line Parameters Estimation Based on Synchronized Measurements," *IEEE Open J. Instrum. Meas.*, vol. 2, pp. 1–11, 2023, doi: 10.1109/OJIM.2023.3250280.
[10] Y. Yuan, S. H. Low, O. Ardakanian, and C. J. Tomlin, "Inverse Power Flow Problem," *IEEE Trans. Control Netw. Syst.*, vol. 10, no. 1, pp. 261–273, Mar. 2023, doi: 10.1109/TCNS.2022.3199084.
[11] J. Zhang, Y. Wang, Y. Weng, and N. Zhang, "Topology Identification and Line Parameter Estimation for Non-PMU Distribution Network: A Numerical Method," *IEEE Trans. Smart Grid*, vol. 11, no. 5, pp. 4440–4453, Sep. 2020, doi: 10.1109/TSG.2020.2979368.
[12] E. L. da C. Saldanha, M. de F. Pacheco, and Â. P. Ferreira, "Estimation of Transmission Line Parameters in Modern Power Systems from Phasor Measurements," presented at the Mediterranen Smart Cities Conference (MSCC 2024), Marroco, 2024.
[13] J. J. Grainger and W. D. Stevenson, *Power System Analysis*. McGraw-Hill, 1994.
[14] A. C. Varghese, A. Pal, and G. Dasarathy, "Transmission Line Parameter Estimation Under Non-Gaussian Measurement Noise," *IEEE Trans. Power Syst.*, pp. 1–16, 2022, doi: 10.1109/TPWRS.2022.3204232.
[15] R. Khalili and A. Abur, "Transmission Line Parameter Error Identification and Estimation in Three-Phase Networks," *IEEE Trans. Power Syst.*, vol. 37, no. 3, pp. 2271–2282, May 2022, doi: 10.1109/TPWRS.2021.3118007.
[16] H. Goklani, G. Gajjar, and S. A. Soman, "Instrument Transformer Calibration and Robust Estimation of Transmission Line Parameters Using PMU Measurements," *IEEE Trans. Power Syst.*, vol. 36, no. 3, pp. 1761–1770, May 2021, doi: 10.1109/TPWRS.2020.3036605.
[17] P. Ren, H. Lev-Ari, and A. Abur, "Tracking Three-Phase Untransposed Transmission Line Parameters Using Synchronized Measurements," *IEEE Trans. Power Syst.*, vol. 33, no. 4, pp. 4155–4163, Jul. 2018, doi: 10.1109/TPWRS.2017.2780225.
[18] Z. Shi, Q. Xu, Y. Liu, C. Wu, and Y. Yang, "Line parameter, topology and phase estimation in three-phase distribution networks with non-μPMUs," *Int. J. Electr. Power Energy Syst.*, vol. 155, p. 109658, Jan. 2024, doi: 10.1016/j.ijepes.2023.109658.
[19] Y. Wang, W. Xu, and J. Shen, "Online Tracking of Transmission-Line Parameters Using SCADA Data," *IEEE Trans. Power Deliv.*, vol. 31, no. 2, pp. 674–682, Apr. 2016, doi: 10.1109/TPWRD.2015.2474699.
[20] S. Kurokawa, J. Pissolato, M. C. Tavares, C. M. Portela, and A. J. Prado, "A new procedure to derive transmission-line parameters: applications and restrictions," *IEEE Trans. Power Deliv.*, vol. 21, no. 1, pp. 492–498, Jan. 2006, doi: 10.1109/TPWRD.2005.852296.
[21] Y. Du and Y. Liao, "On-line estimation of transmission line parameters, temperature and sag using PMU measurements," *Electr. Power Syst. Res.*, vol. 93, pp. 39–45, Dec. 2012, doi: 10.1016/j.epsr.2012.07.007.
[22] M. R. M. Castillo, J. B. A. L. Jr, and N. G. Bretas, "Identification and estimation of power system branch parameter error," in *2009 IEEE Power & Energy Society General Meeting*, Jul. 2009, pp. 1–8. doi: 10.1109/PES.2009.5275219.
[23] M. R. M. Castillo, N. G. Bretas, and J. B. A. London, "Improved branch parameter

errors detection, identification and correction," in *PES T&D 2012*, May 2012, pp. 1–7. doi: 10.1109/TDC.2012.6281590.
[24] M. Asprou and E. Kyriakides, "Identification and Estimation of Erroneous Transmission Line Parameters Using PMU Measurements," *IEEE Trans. Power Deliv.*, vol. 32, no. 6, pp. 2510–2519, Dec. 2017, doi: 10.1109/TPWRD.2017.2648881.
[25] J. B. A. London, L. Mili, and N. G. Bretas, "An observability analysis method for a combined parameter and state estimation of a power system," in *2004 International Conference on Probabilistic Methods Applied to Power Systems*, Sep. 2004, pp. 594–599. Accessed: May 14, 2024. [Online]. Available: https://ieeexplore.ieee.org/document/1378754
[26] M. R. M. Castillo, J. B. A. London, N. G. Bretas, S. Lefebvre, J. Prévost, and B. Lambert, "Offline Detection, Identification, and Correction of Branch Parameter Errors Based on Several Measurement Snapshots," *IEEE Trans. Power Syst.*, vol. 26, no. 2, pp. 870–877, May 2011, doi: 10.1109/TPWRS.2010.2061876.
[27] A. Abur and A. Gómez Expósito, *Power system state estimation: theory and implementation*. in Power engineering. New York, NY: Marcel Dekker, 2004.
[28] W.-H. E. Liu and S.-L. Lim, "Parameter error identification and estimation in power system state estimation," *IEEE Trans. Power Syst.*, vol. 10, no. 1, pp. 200–209, Feb. 1995, doi: 10.1109/59.373943.
[29] M. Asprou and E. Kyriakides, "Estimation of line parameters using the hybrid state estimator," in *2013 IEEE Grenoble Conference*, Jun. 2013, pp. 1–6. doi: 10.1109/PTC.2013.6652160.
[30] Y. Lin and A. Abur, "Enhancing Network Parameter Error Detection and Correction via Multiple Measurement Scans," *IEEE Trans. Power Syst.*, vol. 32, no. 3, pp. 2417–2425, May 2017, doi: 10.1109/TPWRS.2016.2608964.
[31] Y. Liao and M. Kezunovic, "Online Optimal Transmission Line Parameter Estimation for Relaying Applications," *IEEE Trans. Power Deliv.*, vol. 24, no. 1, pp. 96–102, Jan. 2009, doi: 10.1109/TPWRD.2008.2002875.
[32] C. Li, Y. Zhang, H. Zhang, Q. Wu, and V. Terzija, "Measurement-Based Transmission Line Parameter Estimation With Adaptive Data Selection Scheme," *IEEE Trans. Smart Grid*, vol. 9, no. 6, pp. 5764–5773, Nov. 2018, doi: 10.1109/TSG.2017.2696619.
[33] C. S. Indulkar and K. Ramalingam, "Estimation of transmission line parameters from measurements," *Int. J. Electr. Power Energy Syst.*, vol. 30, no. 5, pp. 337–342, Jun. 2008, doi: 10.1016/j.ijepes.2007.08.003.
[34] S.-K. Chai and A. Sekar, "Graph theory application to deregulated power system," in *Proceedings of the 33rd Southeastern Symposium on System Theory (Cat. No.01EX460)*, Mar. 2001, pp. 117–121. doi: 10.1109/SSST.2001.918502.
[35] M. Jorjani, H. Seifi, and A. Y. Varjani, "A Graph Theory-Based Approach to Detect False Data Injection Attacks in Power System AC State Estimation," *IEEE Trans. Ind. Inform.*, vol. 17, no. 4, pp. 2465–2475, Apr. 2021, doi: 10.1109/TII.2020.2999571.
[36] R. Gopalakrishnan, R. Pavithra, D. S. Vidhya, S. Jaividhya, and K. Sethilvadivu, "Phasor Measurement Unit Across the World and Variables Influencing the Cost of Installing a Phasor Measurement Unit," in *2023 International Conference on Sustainable Computing and Data Communication Systems (ICSCDS)*, Erode, India: IEEE, Mar. 2023, pp. 994–999. doi: 10.1109/ICSCDS56580.2023.10104938.
[37] O. Muhayimana, P. Toman, V. Vycital, and V. Jurak, "Design and Verification of a Phasor Measurement Unit Model Using Matlab," in *2023 23rd International*

Scientific Conference on Electric Power Engineering (EPE), Brno, Czech Republic: IEEE, May 2023, pp. 1–6. doi: 10.1109/EPE58302.2023.10149258.
[38] O. Muhayimana and P. Toman, "A Review on Phasor Measurement Units and their Applications in Active Distribution Networks," in *2022 IEEE PES/IAS PowerAfrica*, Kigali, Rwanda: IEEE, Aug. 2022, pp. 1–5. doi: 10.1109/PowerAfrica53997.2022.9905351.
[39] A. G. Phadke and J. Thorp, "HISTORY AND APPLICATIONS OF PHASOR MEASUREMENTS," in *2006 IEEE PES Power Systems Conference and Exposition*, Atlanta, Georgia, USA: IEEE, 2006, pp. 331–335. doi: 10.1109/PSCE.2006.296328.
[40] N. Joshi and A. Khandelwal, "Importance of Phasor Measurement Unit in Modern Power System," in *2023 5th International Conference on Smart Systems and Inventive Technology (ICSSIT)*, Tirunelveli, India: IEEE, Jan. 2023, pp. 23–26. doi: 10.1109/ICSSIT55814.2023.10060942.
[41] "RES670 - Phasor measurement unit | Hitachi Energy." Accessed: Oct. 17, 2023. [Online]. Available: https://www.hitachienergy.com/products-and-solutions/substation-automation-protection-and-control/products/protection-and-control/phasor-measurement/res670
[42] A. Aljazaeri and P. Toman, "A Review of the Use of Phasor Measurement Units in Power System State Estimation," in *2022 22nd International Scientific Conference on Electric Power Engineering (EPE)*, Jun. 2022, pp. 1–6. doi: 10.1109/EPE54603.2022.9814130.
[43] M. Baba *et al.*, "A review of the importance of synchrophasor technology, smart grid, and applications," *Bull. Pol. Acad. Sci. Tech. Sci.*, pp. e143826–e143826, 2022.
[44] A. A. Al Qaralleh, K. Alawasa, and A. I. Al-Odienat, "Optimal Location of PMUs to Enhance State Estimation of Power Systems," in *2023 IEEE Jordan International Joint Conference on Electrical Engineering and Information Technology (JEEIT)*, Amman, Jordan: IEEE, May 2023, pp. 38–43. doi: 10.1109/JEEIT58638.2023.10185724.
[45] "NASPI Synchrophasor Technology Fact Sheet, October 2014 | North American SynchroPhasor Initiative." Accessed: Oct. 25, 2023. [Online]. Available: https://www.naspi.org/node/384
[46] "Big Data Synchrophasor Analysis," Energy.gov. Accessed: Oct. 25, 2023. [Online]. Available: https://www.energy.gov/oe/big-data-synchrophasor-analysis
[47] H. G. Abood, H. Al-Saadi, and G. A. Salman, "Assessing Algorithms of Phasor Measurements Optimal Placement for State Estimation," in *2019 IEEE Conference on Sustainable Utilization and Development in Engineering and Technologies (CSUDET)*, Nov. 2019, pp. 184–187. doi: 10.1109/CSUDET47057.2019.9214675.
[48] A. I. Al-Odienat, B. Malahmeh, and A. R. Tarawneh, "The Optimal PMU Placement in the Power Systems for the Enhancement of State Estimation," in *2020 International Conference on Electrical, Communication, and Computer Engineering (ICECCE)*, Istanbul, Turkey: IEEE, Jun. 2020, pp. 1–6. doi: 10.1109/ICECCE49384.2020.9179214.
[49] M. U. Usman and M. O. Faruque, "Applications of synchrophasor technologies in power systems," *J. Mod. Power Syst. Clean Energy*, vol. 7, no. 2, pp. 211–226, Mar. 2019, doi: 10.1007/s40565-018-0455-8.
[50] D. A. Tziouvaras and D. Hou, "Out-of-step protection fundamentals and advancements," Apr. 2004, pp. 282–307. doi: 10.1109/CPRE.2004.1287097.
[51] D. B. West, *Introduction to Graph Theory*. Prentice Hall, 2001.
[52] C. Godsil and G. F. Royle, *Algebraic Graph Theory*. Springer Science & Business

Media, 2001.
[53] R. Moreno Chuquen and H. R. Chamorro, *Graph theory applications to deregulated power systems*. in SpringerBriefs in Electrical and Computer Engineering. Cham, Switzerland: Springer, 2021.
[54] N. Carter, "Eigenvalues and Eigenvectors of Electrical Networks".
[55] N. R. Shivakumar and A. Jain, "A Review of Power System Dynamic State Estimation Techniques," in *2008 Joint International Conference on Power System Technology and IEEE Power India Conference*, New Delhi, India: IEEE, Oct. 2008, pp. 1–6. doi: 10.1109/ICPST.2008.4745312.
[56] L. Zanni, "Power-System State Estimation based on PMUs: Static and Dynamic Approaches - from Theory to Real Implementation," EPFL, Lausanne, 2017. doi: 10.5075/epfl-thesis-7665.
[57] J. Zhao *et al.*, "Power System Dynamic State Estimation: Motivations, Definitions, Methodologies, and Future Work," *IEEE Trans. Power Syst.*, vol. 34, no. 4, pp. 3188–3198, Jul. 2019, doi: 10.1109/TPWRS.2019.2894769.
[58] J. Vijaychandra, B. R. V. Prasad, V. K. Darapureddi, B. V. Rao, and Ł. Knypiński, "A Review of Distribution System State Estimation Methods and Their Applications in Power Systems," *Electronics*, vol. 12, no. 3, Art. no. 3, Jan. 2023, doi: 10.3390/electronics12030603.
[59] J. Zhu and B. Ramachandran, "Review of Trends in State Estimation of Power Distribution Networks," *J. Power Energy Eng.*, vol. 08, no. 08, pp. 85–99, 2020, doi: 10.4236/jpee.2020.88007.
[60] Y. Liu *et al.*, "Dynamic State Estimation for Power System Control and Protection," *IEEE Trans. Power Syst.*, vol. 36, no. 6, pp. 5909–5921, Nov. 2021, doi: 10.1109/TPWRS.2021.3079395.
[61] "Enhanced Power System State Estimation Techniques for the Incorporation of Variable Energy," Khalifa University. Accessed: May 16, 2024. [Online]. Available: https://khazna.ku.ac.ae/en/studentTheses/enhanced-power-system-state-estimation-techniques-for-the-incorpo-2
[62] A. Sharma and S. Jain, "A Review and Performance Comparison of Power System State Estimation Techniques," May 2018, pp. 770–775. doi: 10.1109/ISGT-Asia.2018.8467861.
[63] G. R. Krumpholz, K. A. Clements, and P. W. Davis, "Power System Observability: A Practical Algorithm Using Network Topology." Accessed: Jul. 21, 2023. [Online]. Available: https://ieeexplore.ieee.org/abstract/document/4113961/
[64] M. Gol and A. Abur, "Observability analysis of systems containing phasor measurements," in *2012 IEEE Power and Energy Society General Meeting*, San Diego, CA: IEEE, Jul. 2012, pp. 1–6. doi: 10.1109/PESGM.2012.6345239.
[65] H. Zhang and K. Han, "A Hybrid Observability Analysis Method for Power System State Estimation," *IEEE Access*, vol. 8, pp. 73388–73397, 2020, doi: 10.1109/ACCESS.2020.2987358.
[66] R. R. Nucera and M. L. Gilles, "Observability analysis: a new topological algorithm," *IEEE Trans. Power Syst.*, vol. 6, no. 2, pp. 466–475, May 1991, doi: 10.1109/59.76688.
[67] R. D. Zimmerman and C. E. Murillo-Sánchez, "MATPOWER." [object Object], Oct. 08, 2020. doi: 10.5281/ZENODO.4074135.
[68] F. Angizeh, A. Ghofrani, and M. A. Jafari, "Dataset on Hourly Load Profiles for a Set of 24 Facilities from Industrial, Commercial, and Residential End-use Sectors," vol. 1, Aug. 2020, doi: 10.17632/rfnp2d3kjp.1.
[69] "IEEE 14-Bus System - Illinois Center for a Smarter Electric Grid (ICSEG)."

Accessed: Feb. 05, 2024. [Online]. Available: https://icseg.iti.illinois.edu/ieee-14-bus-system/

Annex A

Table 26 – Terminal conditions of the IEEE 14 bus system.

Bus	V (pu)	Θ (degrees)	P (MW)	Q (Mvar)
1	1,06	0	114,17	405,43
2	1,045	0	40	0
3	1,01	0	-	-
4	1	0		
5	1	0		
6	1	0	0	-
7	1	0		
8	1	0	0	-
9	1	0		
10	1	0		
11	1	0		
12	1	0		
13	1	0		
14	1	0		

Table 27 – Line parameters for the IEEE 14 bus system.

Line	R (pu)	X (pu)	B (pu)
1-2	0,01938	0,05917	0,0528
1-5	0,05403	0,22304	0,0438
2-3	0,04699	0,19797	0,0374
2-4	0,05811	0,17632	0,0492
2-5	0,05695	0,17388	0,034
3-4	0,06701	0,17103	0,0346
4-5	0,01335	0,04211	0,0128
4-7	0	0,20912	0
4-9	0	0,55618	0

5-6	0	0,25202	0
6-11	0,09498	0,1989	0
6-12	0,12291	0,25581	0
6-13	0,06615	0,13027	0
7-8	0	0,17615	0
7-9	0	0,11001	0
9-10	0,03181	0,0845	0
9-14	0,12711	0,27038	0
10-11	0,08205	0,19207	0
12-13	0,22092	0,19988	0
13-14	0,17093	0,34802	0

Table 28- Load characteristics for the IEEE 14 bus system.

Bus	**P (MW)**	**Q (Mvar)**
2	21,7	12,7
3	94,2	19,1
4	47,8	-3,9
5	7,6	1,6
6	11,2	7,5
9	29,5	16,6
10	9	5,8
11	3,5	1,8
12	6,1	1,6
13	13,8	5,8
14	14,9	5

Annex B

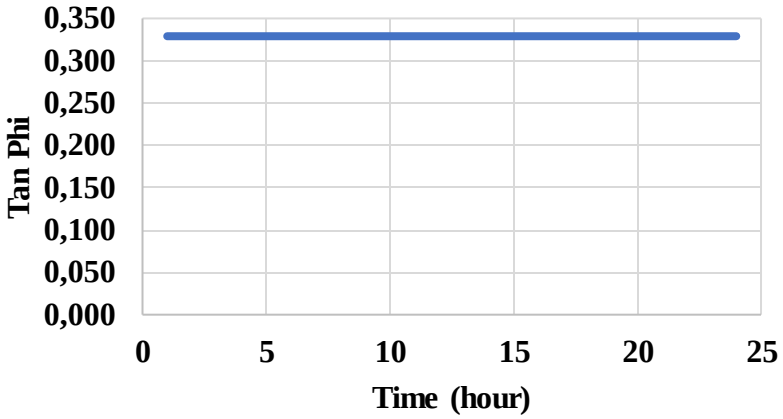

Figure 52- Tangent of Phi of load 2 through time.

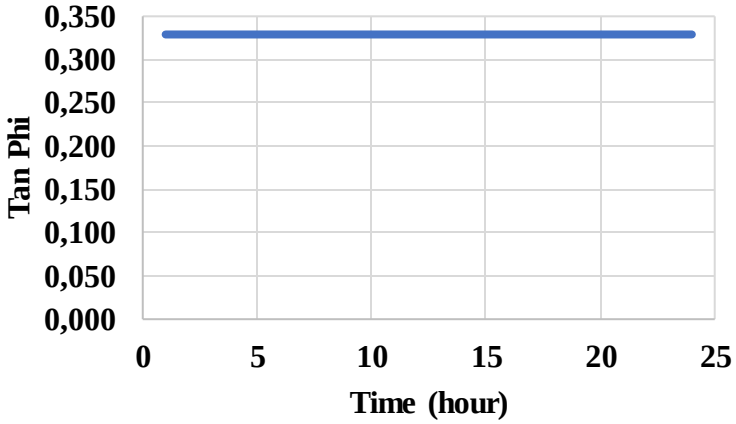

Figure 53- Tangent of Phi of load 3 through time.

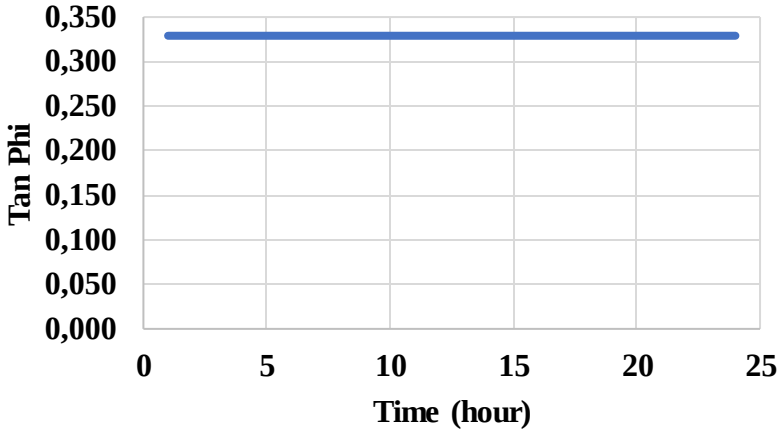

Figure 54- Tangent of Phi of load 4 through time.

Annex C

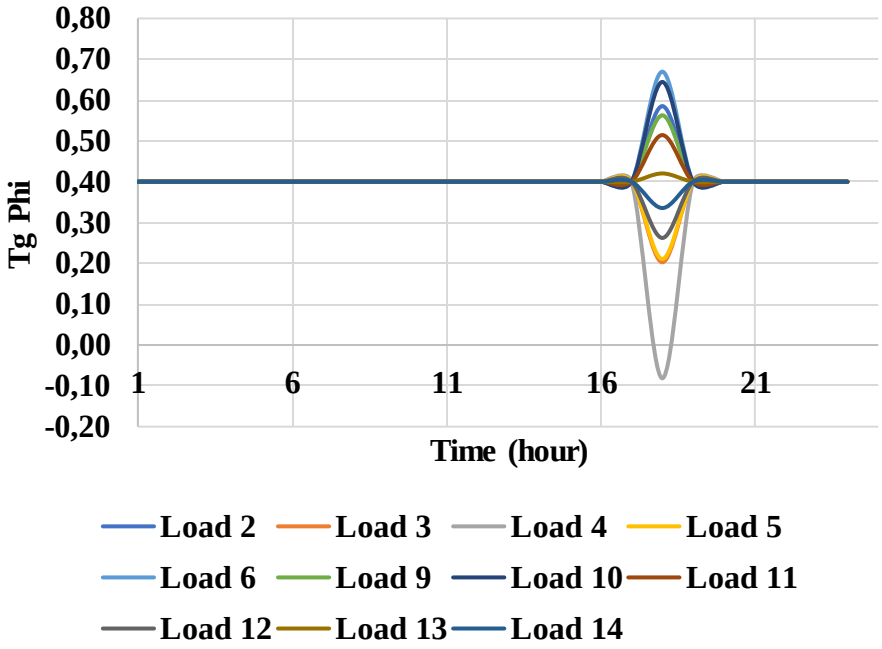

Figure 55 – Tangent phi of the loads through time.